DEPARTMENT OF PHYSICS
UNIVERSITY OF JYVÄSKYLÄ
LABORATORY REPORT No. 6/2003

ELASTICITY AND STIFFNESS EVOLUTION IN RANDOM FIBRE NETWORKS

BY
SAMI KÄHKÖNEN

Thesis for the Degree of
Licentiate of Philosophy

Jyväskylä, Finland
October 2003

Preface

This work has been carried out during the years 2001-2002 at the University of Jyväskylä, Department of Physics. I would like to express my gratitude to professor Jussi Timonen and Dr. Jan Åström for guidance and for introducing me to this subject. Thanks goes also to Sanna for love and support.

In Jyväskylä, 28 October 2003

Sami Kähkönen

Kähkönen, Sami
Elasticity and stiffness evolution in random fibre networks
University of Jyväskylä, 2003, 56p.
(Laboratory Report/Department of Physics, University of Jyväskylä
ISSN 0357-9344; 6/2003)
ISBN 951-39-1621-9
Licentiate Thesis

Supervisors:
Professor Jussi Timonen, University of Jyväskylä, Finland
Dr. Jan Åström, University of Jyväskylä, Finland
Reviewers:
Professor Kai Nordlund, University of Helsinki, Finland
Docent Mikko Karttunen, Helsinki University of Technology, Finland

Abstract

The great tragedy of Science - the slaying of a beautiful hypothesis by an ugly fact.
- Thomas H. Huxley (1825 - 1895)

This thesis deals with geometrical, statistical and mechanical properties of random line (fibre) networks. It begins with an introduction to elasticity theory and various properties of random fibre networks. The main body of the thesis consists first of all of a review of a new mean field theory for the elasticity of random three dimensional networks of fibres. This theory agrees very well with the results of direct numerical simulations for a fairly wide range of parameters. An essential feature in this theory is the connectivity of the network, i.e. the average number of contacts per fibre, which together with the properties of individual fibres completely determines the elasticity, and also the porosity, of the network. The theory has been generalised to three dimensions by determining numerically the ratio of apparent contacts which appear in the two dimensional projection of the three dimensional structure. Also in this case agreement with direct numerical simulations is found to be very good. Extension of the theory to other disordered structures, e.g. granular packings, is possible

Thereafter a 'stiffness evolution' in two dimensional networks of elastic beams (fibres) will be considered. As a first attempt, the evolution strategy is chosen such that mass is moved from the least elastic energy containing segment to the most energetic one, and the process is then iterated. Evolution of stress bearing structures is then followed under constant elastic load. Results and a minimal analytical model are given for applied tensile and shear stress. We find e.g. that for low density networks the developing stress bearing structure becomes localised around a single path for applied tensile (shear) stress, while the structure becomes less localised for increasing density of the network.

Contents

Chapter 1

Introduction

The elastic properties of any material depend upon the details of its structure. The purpose of this thesis is to understand macroscopic properties of random networks in terms of their constituents and their mutual interactions.
The first one to consider the properties of fibrous structures based on their constituents and orientation was Cox [4]. Random fibre materials offer interesting means for building materials with a wide variation of properties for different applications. Airplanes and sailboats are made of glass fibre mats, as strong and yet light structures are needed. Ordinary copy paper made of wood fibres is another example where material stiffness and strength are important, but in this case it is perhaps permeability which is even more important, as it is related to the drying and printability of paper [5]. Also, evolution seems to favour fibrous materials (more discussion on this in Ch. 5). The structure of human bone, for example, is to a large extent of this kind. An interesting feature of human bone is that it can adapt its material distribution to the external load conditions. An athlete, with specialised type of training, develops a different kind of bone structure than an astronaut who has spent a long time at zero gravity (i.e. zero load enviroment). A disturbance in the adaptive bone mechanism leads to a condition of weakening bones which is known as osteoporosis.
This thesis is a continuation and related to the work previously done in the Department of Physics [20,27,25] in the area of random fibrous structures. Dr. Kellomäki concentrated in his work [20] on wave dynamics of random fibre and random spring networks, and Dr. Latva-Kokko considered the rigidity of randomly structured materials. This work is mainly a continuation to the work of Dr. Mäkinen, as we deal with the elastic properties of fibre mats, and then extend the topic to stiffness evolution.
The reason for studying the present topic is that materials of practical interest rarely are perfect, and sometimes structural disorder is even desirable. Perfect materials are hard to manufacture, while introducing controlled disorder is much easier. Disorder appears in many different scales, from the atomistic

scale (as e.g. in a crystal structure) to the macroscopic scale (as e.g. in composite materials). The usual way to describe a material with imperfections is by *homogenization*, i.e. the properties of the material are described statistically as those of a homogeneous material, i.e. averaged over certain volume element. Thus it is possible e.g. to describe the random fibre network as an *effective medium* as described in detail in Sec. 3.2.

1.1 Outline of the thesis

In Ch. 2 I present an overview of the properties of two-dimensional random fibre networks together with a comparison with random resistor networks. In the following Ch. 3, the two-dimensional (2d) case is generalized to three dimensions. Furthermore, in Ch. 4 the effective medium model as presented in Sec. 3.2.2 is extended to the porosity of the fibre network. In this way elasticity and porosity are both found to be dependent on the connectivity of the material. In Ch. 5 I consider the stiffness evolution in a 2d fibrous structure. A simple analytical model is presented together with some statistical properties that follow from it. In the last Ch. 6 I summarize and discuss the results obtained.

1.2 Basics of elasticity theory

I give here a short summary of elasticity theory as it is widely used in the rest of the thesis. The basic equations of elasticity theory were formulated already a long time ago by Cauchy and Poisson, for the description of the mechanics of continuum media [23].

An elastic material is one that responds to an applied external force by deforming and returns to its original shape upon removal of this force. Elastic behaviour thus precludes permanent deformation. Elasticity can be linear or nonlinear. In the linear case, the deformation is proportional to the external force used. In the following I consider only linear deformations.

We begin by defining the *strain* tensor through derivatives of the displacement vector u_i [24],

$$u_{ij} = \frac{1}{2}\left(\frac{\partial u_i}{\partial x_j} + \frac{\partial u_j}{\partial x_i} + \frac{\partial u_k}{\partial x_i}\frac{\partial u_k}{\partial x_j}\right), \tag{1.1}$$

where the suffixes i and j run through coordinate indexes.

The strain tensor gives the change in the local length units when the system is deformed. By considering only small deformations in the linear regime we can neglect the last term in Eq. (1.1) because it is of second order. Thus the strain

tensor can be written as

$$u_{ij} = \frac{1}{2}\left(\frac{\partial u_i}{\partial x_j} + \frac{\partial u_j}{\partial x_i}\right). \tag{1.2}$$

The basic assumption of a linearly elastic material is the generalised Hooke's law,

$$\tau_{ij} = C_{ijkl} u_{kl}, \tag{1.3}$$

with τ_{ij} the *stress* tensor and C_{ijkl} the material constants (elastic stiffness contants or elastic moduli). In principle we have 81 $(= 3^4)$ different constants. Because the stress and strain tensors are both symmetric, one finds that $C_{ijkl} = C_{jikl}, C_{ijkl} = C_{ijlk}$, and, by energy considerations, $C_{ijkl} = C_{klij}$. Thus C finally has only 21 linearly independent elements.

If the material constants do not depend on the space variables, the material is said to be *homogeneous*. Also, if the elastic moduli do not depend on the choice of the coordinate system, the material is said to be *isotropic*. For homogeneous, isotropic materials the number of elastic moduli reduces to just two, and Eq. (1.3) can be written in the form

$$\tau_{ij} = \lambda \sigma_{ij} u_{kk} + 2\mu u_{kl}, \tag{1.4}$$

where λ and μ are the Lamé coefficients[1]. More widely used (e.g. in engineering) elastic constants are Young's modulus E and Poisson's ratio σ,

$$\mu = \frac{E}{2(1+\sigma)}, \quad \lambda = \frac{E\sigma}{(1+\sigma)(1-2\sigma)}. \tag{1.5}$$

Notice that for mechanical stability $\lambda, \mu, E > 0$, and $0 < \sigma < \frac{1}{2}$. The mechanical stability means that there exists an inverse of the generalized Hooke's law so that we can calculate the components of the strain tensor from the stress tensor [28]. One reason for using the parameters E and σ is that they have a clear physical interpretation; Young's modulus describes how much force is needed to attain a given deformation while Poisson ratio is the ratio of transverse compression and the longitudinal extension.

The equilibrium condition for an isotropic body can be written in the form [24]

$$(1-2\sigma)\frac{\partial^2 u_i}{\partial x_k^2} + \frac{\partial^2 u_l}{\partial x_i x_l} = 0, \tag{1.6}$$

and the external forces appear in the solution only through boundary conditions.

Considering only an extension or a compression of a body, we get the follow-

[1] $\lambda = C_{1122}$ and $\mu = C_{1212}$.

ing relation by using Eqs. (1.2), (1.4) and (1.5),

$$\tau_{xx} = E u_{xx}, \tag{1.7}$$

where elongation is along the x-axis. If Poisson contraction is prohibited in the y-direction, we get

$$\tau_{xx} = \frac{E}{(1-\sigma^2)} u_{xx}. \tag{1.8}$$

With similar reasoning from the same equations, we get for the shear deformation of a body

$$\tau_{xy} = \frac{E}{2(1+\sigma)} u_{xy}. \tag{1.9}$$

Consideration of a more general theory instead of the rather simple assumptions of linear elasticity and Hooke's law, would bring us to the so called *Cosserat elasticity*. Cosserat elasticity is said to be the most general elasticity theory that fulfills the Galilean invariance[2]. The displacement field of a *rigid solid* in three dimensions can be characterized by translation and rotation, i.e. by six degrees of freedom by introducing two strain fields which both will respect the Galilean invariance. The strain is given by $\varepsilon_{ij} = \partial_{ij} U_j - \epsilon_{ijk}\varphi_k$, where U is the displacement field, φ is the rotation field, and ϵ is an antisymmetric tensor[3]. There is a minus sign in front of the rotation field so that the strain remains invariant under rigid rotation. The rotation field also determines the torsion field κ such that $\kappa_{ij} = \partial_i \varphi_j$. From the theory it is possible to obtain a length scale for rotations. Above this scale, rotations have no meaning, the additional terms should vanish and only the displacement field is needed [14]. Different deformation modes regarding the individual building blocks of a random fibre mat were considered in [50], and the rotations were shown not to contribute to the elastic properties of the mat. Therefore, there is no need for more general theory and we can neglect the rotation field introduced by Cosserat elasticity.

[2]Galilean invariance implies that the stress field should not do any work under rigid motion of a solid.

[3]An antisymmetric (also called alternating) tensor is a tensor which changes sign when two indices are interchanged.

Chapter 2

Two-dimensional random fibre networks

Most of the research on the elastic deformation of disordered media is done on lattice models with ad hoc disorder. Other models include bond-bending and beam models. Often electrical random fuse network models are used as an analogy to elasticity. The elasticity versus electricity aspect is studied in more detail in Sec. 2.3.1. In the following section we present the basic construction method of a random fibre network, and its percolation and statistical properties are considered as a consequence of the forming process. In Sec. 3 we extend this model to three dimensions for which an effective medium approach is considered together with some transport properties.

2.1 Introduction

As a model for a random porous medium we use here a random network of lines. Images of networks with different parameters are given in Fig. 2.1 below. A random fibre network is defined as an independently deposited system of finite-length lines on a two-dimensional plane. We construct our network by depositing fibres of length L_f on a plane whose area is defined by $L_x L_y$, and which has periodic boundaries in the y-direction.
The two-dimensional random line network thus constructed is a geometrical structure. At every point where two fibres cross they are assumed to be rigidly bonded to each other. The midpoints and the orientations of the fibres are chosen from uniform uncorrelated distributions, the orientation angles from the interval $[-\pi/2, \pi/2]$, and the midpoints are uniformly distributed in the square spanned by lengths $L_x + L_f$ and $L_y + L_f$. The side lengths of the square have been increased by L_f because we want to avoid the density of fibres to be lower at the boundaries of the square defined by $L_x \times L_y$. For small numbers of fibres the system is not connected. With increasing coverage the system reaches the

geometrical percolation threshold (more on this in Sec. 2.2) at $q_c \equiv 5.71$ fibres per unit area (with unit fibre length), and the system becomes connected. By assuming that between the fibre-fibre bonds (nodes) there are central-force springs, a geometrically connected network does not necessarily have a nonzero stiffness. As a central-force network consists of both rigid (triangles) and non-rigid (more than three-sided polygons) structures, the average coordination number (see Table 2.1) never exceeds four, and random spring networks have thus zero stiffness at any finite coverage. So the stiffness of a random fibre network relies totally on a nonzero stiffness of all deformation modes (axial, shear and bending) of an individual segment.

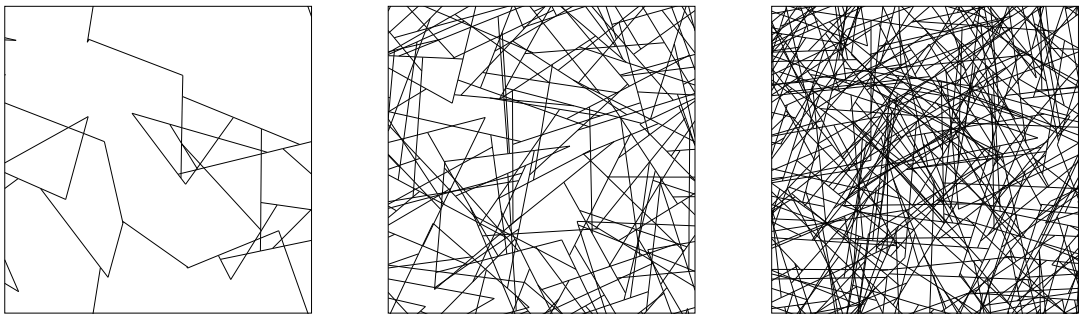

Figure 2.1. Examples of random line networks in an area of 2.1×2.1 with $L_f = 1$, for densities $q/q_c = 1, 4$ and 9 from left to right, respectively. Dangling ends are removed.

2.2 Percolation and statistical properties

The specific process which is used to create the network depicts also many of its properties. In the following we will study them more closely. We study properties which *percolate* from one side of the system to the opposite side like connectivity and rigidity. Percolation is applied in many different fields of science like communication, biology and physics. Applications extend from fluid flow in a porous medium and current flow in a metal-insulator system to forest fires and diffusion. The wide variety of applications arises from the fact that percolation is a generic model for spatially random processes [14]. As a model for a disordered medium, percolation is also one of the simplest and yet a powerful method that provides realistic and qualitatively good predictions for random media. This is especially true in the field of phase transitions in random networks.

Geometrical connectivity-percolation was studied by Pike and Seager [34, 39] using computer simulations. The percolation threshold considered by them was the critical line length when there is a connected spanning cluster in the thermodynamic limit $L \to \infty$, and they found a critical line length that corresponds to the (dimensionless) critical percolation density $q_c = 17.94/\pi = 5.71$. Other properties of the 2d random line network are summarized in the following Table 2.1, where N_f is the total number of fibres, L_f the length of a fibre and A the area of the network.

Total length of fibres	$L = N_f L_f$
Density of fibres (dimensionless)	$q = N_f L_f^2 / A$
Connectivity percolation density	$q_c = \frac{17.94}{\pi} = 5.71$
Number of crossing points between fibres	$N_c = \frac{\left(N_f L_f\right)^2}{\pi A}$
Average number of crossing points per fibre	$\bar{c} = \frac{2N_c}{N_f} = \frac{2N_f L_f}{\pi A}$
Average distance between crossing points	$\hat{\ell} = \frac{L_f}{\bar{c}} = \frac{\pi L_f}{2q}$
Average number of sides in a polygon	$N_s = 4$
Number of polygons	$N_h = (N_c - N_f) e^{-N_f \bar{\alpha}/A}$

Table 2.1. Properties of the 2d random fibre (line) network.

Because both the angle and the centre-point distributions are uniform, we get a Poisson distribution for the segment-length distribution,

$$\sigma(\ell) = \hat{\ell}^{-1} e^{-\ell/\hat{\ell}}, \tag{2.1}$$

where $\hat{\ell}$ is the average segment length. By introducing a dilution factor a, which satisfies $0 < a < 1$, we can change the frequency of the Poisson process. Now the average segment length becomes $\hat{\ell} = \pi L_f/(2aq)$. This result can be used to describe the situation where some of the bonds are diluted.

2.3 Rigidity percolation

A system is said to be rigid if it cannot be deformed without changing its energy. Rigidity of a system can be checked by *a)* implying a nonzero deformation to the equilibrium configuration of the system, i.e. changing the boundary conditions and solving the resulting set of elastic equations of the system, *b)* considering the degrees of freedom and the constraints [26] or *c)* using graph theory and matching algorithms [16].
In the first case we try to find if there is a definite response to a given deformation. Under positive response the system is rigid, otherwise not. Moreover, we can check the system only in one direction at a time, thus this method is time consuming if we want to study the behaviour in more than one direction.

Constraint counting considers rigidity as a static property as opposed to direct solving of the elastic equations, where rigidity is seen as a dynamic property. Now by defining a floppy mode as a motion which costs no energy, and assuming that each constraint removes one floppy mode[1], we can examine constraint counting more closely. For any system (rigid or non-rigid) in d dimensions, there exists d translations and $\binom{d}{2}$ rotations. From the translations of N mass points we get Nd degrees of freedom. So the number of floppy modes in d dimenions with N_c linearly independent constraints is

$$F = Nd - N_c - \left(d + \frac{d(d-1))}{2} \right). \tag{2.2}$$

This method is called Maxwell counting. If we increase the number of constraints gradually, the number of floppy modes F found in this way becomes zero at some concentration of bonds. It is assumed that at this point the network becomes rigid as a whole (rigidity percolation occurs). Unfortunately Maxwell counting is only approximate because some constraints are redundant and they do not change the number of floppy modes. In addition, F is not zero at the rigidity percolation transition because there are floppy inclusions even if the network contains an infinite rigid cluster, so the transition point is determined inaccurately.

Unlike in the methods based on static and dynamic properties of the system, with matching algorithms we try to characterize the system based on the concept of generic rigidity. A system might be rigid for some deformation but not for others. These so called geometric singularities are possible when some collective motions are allowed. A system is generically rigid if it is rigid in almost all possible configurations given by the set of constraints. There might be certain special configurations in which rigidity is not assured, but they must have zero measure in the probability space of all possible configurations.

For example, a system consisting of sites which occupy the corners of a square and are connected by bonds along the sides of the square, is not rigid under shear. The same is true for a chain of collinear bonds which can buckle. For two dimensions there is the so called *Laman's theorem* based on graph theory, which is sufficient for ensuring the generic rigidity of a generic network. However in higher dimensions the theorem is necessary but not sufficient. Based on Laman's theorem there are so called matching algorithms [13] which can be used to identify all rigid clusters in the system. One version of this algorithm is the 'pebble game' [16].

[1] i.e. we assume that all constraints are linearly independent and each binds one degree of freedom

2.3.1 Random fibre network vs. Random resistor network

Scalar percolation [40] is a simple model used for describing the behaviour of a scalar conserved quantity, e.g. an electric charge across a random diluted system, as first suggested by de Gennes [10] in relation to the elasticity of gels. Since then the problem of elasticity of random percolating systems was viewed as analogous to the problem of electrical conductivity, until Feng and Sen [8] showed that it was not generally true. In addition, they suggested that the central-force elastic percolation belongs to a new universality class. More precisely, if the conductivity vanishes at the geometric percolation concentration p_c as $\sigma \sim (p - p_c)^t$, and the elastic modulus as $\sim (p - p_c)^f$, then the prediction by de Gennes is that $f = t$, and by Feng and Sen that $f \neq t$ [48,8,19].

In order to look more closely into this matter, we start by defining the kind of networks we are dealing with. The elastic forces between the nearest neighbours give rise to a random network of elastic bonds. In the framework of the Born model, we can write the Hamiltonian of the microscopic elastic energy as [10,8,19,8]

$$H = \frac{1}{2} \sum_{i,j(nn)} K_{ij} \left[\alpha(\vec{u}_i - \vec{u}_j)_{\parallel}^2 + \beta(\vec{u}_i - \vec{u}_j)_{\perp}^2 \right], \tag{2.3}$$

where (nn) denotes nearest neighbours, $(\vec{u}_i - \vec{u}_j)_{\parallel}$ is the relative displacement of site j in the direction parallel to the bond (i,j), $(\vec{u}_i - \vec{u}_j)_{\perp}$ is the relative displacement in the perpendicular direction and K_{ij} is a random variable which assumes values 1 and 0 with probabilities p and $1-p$, respectively. The Born model (Eq. (2.3)) is a useful model which gives qualitatively correct results in many instances [21]. In the case of purely isotropic Born model, i.e. when $\alpha = \beta$, Eq. (2.3) reduces to a scalar problem, and so to the usual universality class of conductivity problem, as predicted by de Gennes. On the other hand when $\alpha = 1$ and $\beta = 0$, the Hamiltonian in Eq. (2.3) represents a random network of springs, i.e. forces are involved only when a bond stretches or contracts. This model does not reduce to a scalar problem and the analogy with electrical networks is no longer evident. The Born model gives wrong results for example for systems composed of long thin rods, and a solution for this system is proposed in [19] as a new model for elasticity of percolating lattice networks.

Summarizing, if angular forces are present, as opposed to central-force networks, only a singly connected path is required to make the system rigid. Important is also the question raised in [48] that in what kind of stressed elastic network is the de Gennes prediction exactly valid? This subject of classification of rigidity percolation in different kinds of networks (in and off-lattice, stressed, tension free, at zero or at finite temperature) has drawn lately a con-

siderable amount of interest [6,7,18,16,48,8,19,32,16,20,25,34,39,41,45,38].

Chapter 3

Random networks of elastic beams

3.1 Introduction

Rigidity does not address the question of system's response to a deformation or of the strength of the response. In a rigid system its constituents are in fixed positions with respect to one another. If the system can be deformed without cost of energy, it is not rigid.
Three-dimensional mats of randomly (in 2d) oriented fibres can be formed by sedimenting flexible fibres in a random and uncorrelated fashion on a flat substrate. The fibres are originally straight, horizontal, and deposited from above. When a depositing fibre first comes into contact with a fibre below, it bends by an angle ϕ on both sides of the contact (Fig. 3.1(A)).

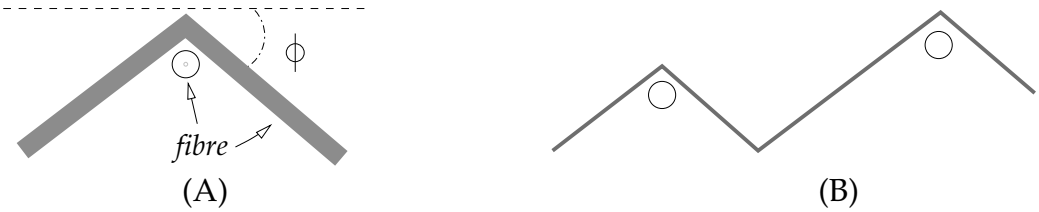

Figure 3.1. A)Definition of the bending angle ϕ and B) an example of bending of a fibre between two crossing fibres.

It can thus come into contact with another fibre, where a similar bending is performed until the fibre end or the substrate is reached. At the end of the fibre an end-node is created, and in the case of the fibre hitting the substrate a bending-type of node is created whereafter the rest of the fibre lies flat on the substrate. The fibre must also bend in between two crossing fibres (Fig. 3.1(B)) in such a way that it can fulfil at both crossings the bending rule shown in (Fig. 3.1(A)). The final result of this deposition process is a kind of zig-zag pattern formed by the fibres as shown in Fig 3.2.
The contacts are assumed to be stiff and all internal stresses formed during the sedimentation process are assumed to vanish. When the angle ϕ approaches

Figure 3.2. A schematic representation of the zig-zag pattern formed by a fibre in the fibre mat. Parameter w_o is a typical segment length and the thickness of the structure is indicated.

zero, a fibre mat is simply a pile of sticks, which obviously has a high porosity. Consequently, as the angle ϕ increases, the porosity will decrease. This aspect of the random fibre network is examined in more detail in the following chapter.

Because the deposition process is very similar to that of the two-dimensional version (now the width of lines is counted) as introduced in Sec. 2.2, the other geometrical and statistical properties of the 3d fibre networks are pretty much the same as for the 2d version. This kind of deposition process obviously pro-

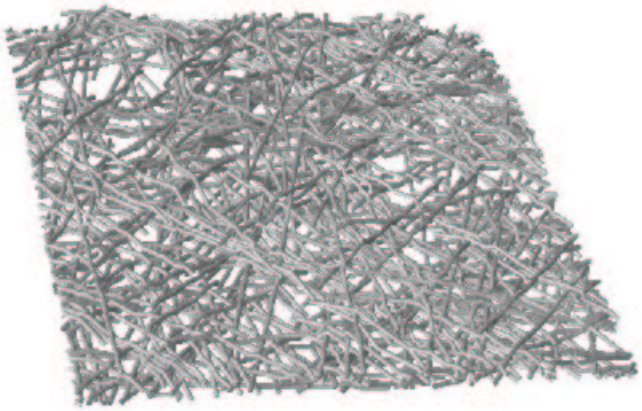

Figure 3.3. A three-dimensional random fibre mat, $q/q_c = 10$, $L_f = 1.0$, $w = 0.02$ and $\phi = 0.3$. See Sec. 3.2.2 for explanation of the terms.

duces a rough surface, but the surface properties are out of the scope of this thesis. For discussion of rough surfaces produced by a similar KCL-PAKKA model see [42].

As implied, our model is similar to the lattice-based PAKKA model [30, 12, 42, 29, 36]. The PAKKA model was developed to study the three-dimensional network structure of paper. In this model flexible fibres are deposited in the same way as in our model, but the bending rules on contacts with other fibres are somewhat different, and bending is of course discrete as the system is defined on a square lattice. Bending is governed by a dimensionless parameter called the bending flexibility number $F = Tw_f/t_f$, where T is the actual flexibility, w_f

the width of the fibres, and t_f the thickness of the fibres. F gives the largest allowed vertical deflection of the fibres from one lattice cell to the next. The PAKKA model only describes the geometrical structure of the system, while our model [52] decribes a fully elastic network of flexible fibres.

3.2 Mechanical properties

To analyze the stress-transfer mechanisms in random fibre networks it is useful to study the stress distribution in the segments. In the fracture of random media the stress distributions can be used to calculate the initial failure process as this process is uncorrelated [14].
Simulations [53] reveal that in this particular kind of network, the distribution of segment stresses can be separated into two different distributions of different physical origin. Figure 3.4 a) shows the segment stress distribution $(P(\sigma))$ averaged over 10 runs [53]. In general, it can be said that in the case of tensile stress in the x direction, in each segment of the network the x component of the stress must be positive and the y component must average to zero due to periodic boundary conditions in that direction.
There is thus a local positive compensation for any negative stress, and this compressive deformation distribution (P_s) must be symmetric as the compressive part of the total stress distribution $(\sigma < 0)$ describes it unambiguously. The remaining load-bearing distribution (P_t) of positive stresses can be parametrized in the form [53]

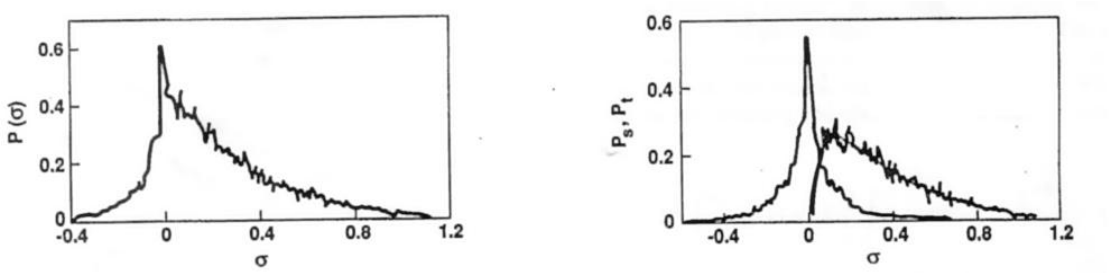

(a) (b)

Figure 3.4. (a) Distribution of axial segment stressess and (b) its splitting into separate distributions P_t and P_s [53].

$$P_t(\sigma) = \Theta(\sigma)\frac{A}{\sigma_t \Gamma(m)}\left(\frac{\sigma}{\sigma_t}\right)^{m-1} e^{-\sigma/\sigma_t}, \tag{3.1}$$

where σ_t is the width of the distribution, A is a normalization constant, Θ is the unit step function, Γ is the gamma function and m is a constant which depends on density and L_f/w. The compressive deformation stresses and their positive

compensation can be parametrized as

$$P_s(\sigma) = \frac{B}{2\sigma_s} e^{-|\sigma/\sigma_s|}, \tag{3.2}$$

where σ_s is the width of the distribution and B is a normalization constant. Using Eqs. (3.1) and (3.2), the whole segment stress distribution is given by

$$P(\sigma) = P_t + P_s = \Theta(\sigma)\frac{A}{\sigma_t \Gamma(m)}\left(\frac{\sigma}{\sigma_t}\right)^{m-1} e^{-\sigma/\sigma_t} + \frac{B}{2\sigma_s} e^{-|\sigma/\sigma_s|}, \tag{3.3}$$

which is normalized such that $A + B = 1$.

This kind of stress distribution in random line networks was first noted in [53], and in [20] for a random network composed of springs. In the case of spring networks under global compression, the total stress distribution was symmetric.

The basic quantities which describe the mechanical behaviour of a system are its elastic moduli. In the case of tensile stress the relevant modulus is the Young's modulus. Effective-medium theories and numerical results indicate that the Young's modulus of 2d random fibre networks is asymptotically a linear function of the areal density (q),

$$E_e(q) = A(q - q_{min}), \tag{3.4}$$

where E_e is the effective Young's modulus, A is a constant, and q_{min} is a 'critical' density that depends on the percolation treshold and the stress transfer mechanism. Close to the percolation treshold q_c one finds a scaling regime, as expected, similarly to other transport properties, and for $q \gg q_c$ (high coverage) the system is in the linear regime. This kind of phenomenon can be demonstrated experimentally in hand-made sheets of paper [37, 35]. The dependence of q_{min} on the percolation threshold is due to the fact that the network has to be geometrically connected for it to be able to carry load. The other elastic moduli of the system can be deduced from continuum elasticity theory (see below).

Next we introduce the Cox model [4] and its variant, the shear-lag model [33], and then introduce a qualitatively new effective-medium model [50]. The shear-lag model suggests that q_{min} should be dependent on the length of the fibres used, L_f, which is not supported by experiments. Also it gives the prefactor A at best qualitatively. The variation of the average stress with respect to fibre orientation, as given by the shear-lag model, seems to be correct, and it is also used in the new effective-medium model. This latter model tries to overcome the shortcomings of the Cox model, and its variant.

3.2.1 Cox model and its variants

In the Cox model we assume that a single fibre is attached to a homogeneous background with full effective stress transfer between the fibre and the background. The stress-strain behaviour of both the fibre and the background are assumed to be linear. The *shear-lag* model differs from the Cox model by introducing a finite length for the fibres, while in the Cox model the fibres extend from one side of the system to the other. The shear-lag model in particular assumes that stress is transferred to fibres through fibre crossings, see Fig. 3.5 [4]. Usually a fibre will lie at an angle θ with respect to the direction of tensile stress

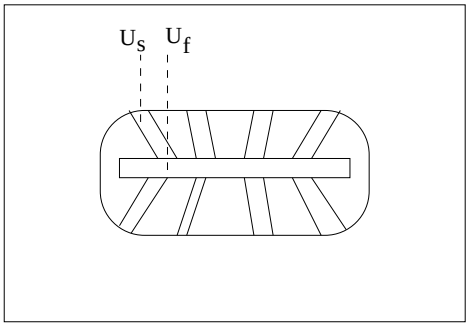

Figure 3.5. Connection of a fibre to the effective medium in the Cox/shear-lag model.

in a homogeneous medium, so we will first consider the case without angular dependence, and return to this dependence afterwards. In the small strain limit we can write a differential equation for the stress (σ_f) along a fibre as

$$\langle l_s \rangle \frac{d\sigma_f}{dx} = c \frac{u_f - u_s}{\langle l_s \rangle}. \tag{3.5}$$

Here u_f and u_s are the local displacements of the fibre and of the backgound as shown in Fig. 3.5, $\langle l_s \rangle$ is the average segment length and factor c is a stiffness constant. Because we assumed linear elasticity in the limit of small strain, the stresses and strains are related through $\sigma = E\epsilon$, where E is the Young's modulus of the fibre. Using this, it is easy to verify that the stress along the fibre, i.e. the solution of Eq. (3.5), is given by

$$\sigma_f(x, k) = E\epsilon_x \left(1 - \frac{\cosh[k(\frac{1}{2} - x/L_f)]}{\cosh(k/2)} \right), \tag{3.6}$$

with $k = \sqrt{c} L_f / \langle l_s \rangle$, and ϵ_x is the strain in the x direction. We can now take into account also the effect of fibre orientation. By assuming isotropic angular distribution for fibres, and in the absence of transverse Poisson contraction, a

rotation of the infinitesimal field σ_f gives

$$\sigma_f(x,\theta) = \sigma_f(x)\cos^2\theta, \tag{3.7}$$

where θ is the angle of the fibre with respect to the external strain.
The elastic modulus of the network is found by integrating over the angle θ and the axial coordinate x along the fibre. In the Cox model we consider a fibre network, where each line extends across the whole system. In this case we get for the Young's modulus per unit thickness [4]

$$E_e = \frac{1}{3}EA_f q, \tag{3.8}$$

where E is the axial Young's modulus of the fibre, A_f is the cross-sectional area of the fibre and q is the total fibre length per unit area.
In the case of the shear-lag model we have fibres of finite length, and stress transfer happens between the nearest segments, i.e. by the *shear-lag mechanism*, while in the Cox model there was no interaction between the fibres, only with the background. The shear-lag model gives [33]

$$E_e = \frac{3}{8}EA_f(q - Kq_c), \tag{3.9}$$

where constant K is $\pi/5.71\sqrt{1+\sigma}$ with σ the Poisson contraction of the fibres. The last term in Eq. (3.9) is due to stress vanishing at the fibre ends. There is also a variant of the shear-lag model with elastic bonds [35].

3.2.2 The effective-medium model

As in the Cox model we begin by considering a single unit attached to a homogeneous background. We do not however treat the fibres as the basic units of the network, nor do we try to describe the stress distribution along them. By doing so we would make the segment stresses correlated along the fibres. In the shear-lag model based on fibres of finite length, there is an explicit contribution in the effective Young's modulus as a consequense of the assumed stress transfer mechanism (the constant K in Eq. (3.9)). This assumed stress transfer mechanism is wrong, as it predicts that the stress is transferred to a fibre at its ends and thus leads to an incorrect density dependence. The shear-lag model also underestimates the elastic energy of segments aligned perpendicular to the external system [37].
Instead of investigating the stress transfer in a whole fibre, we concentrate on a single segment. As explained in Sec. 2.2, the segment length distribution is Poissonian. An effective-medium theory of the elasticity of the network can be based on this additional piece of information. Yet another ingredient of the

effective-medium model of Refs. [50, 52, 51] is that the segments of fibres are assumed to deform only in the most energetically favourable mode depending on their length.

When a fibre network is deformed there must be a force equilibrium at each node. Each of the segments can deform by stretching, bending and shearing. For fibres of square cross section the bending stiffness is Ew^4/l^3, the shear stiffness is $Ew^2/\big(2(1+\sigma)l\big)$ and the tensile stiffness is Ew^2/l. When the length of the segment is much larger than its width (slender segments), bending is the preferred mode of deformation. For small l, however, stretching and shearing are preferred. We can simplify this behaviour by assuming that there is a cut-off length l_c above which the only deformation mode is bending, and below which the segment is only deformed by stretching and shearing. A rough qualitative argument gives $l_c = w\sqrt{2(1+\sigma)}$, which suggests seeking l_c numerically in the form $l_c = (\mathrm{const}_a + \mathrm{const}_b w)\sqrt{2(1+\sigma)}$, with the result that $\mathrm{const}_a = 0.11$ and $\mathrm{const}_b = 1.9$ [52].

To determine the stiffness of the network we still need to quantify the orientation dependence of the local displacements. We show in Fig. 3.6, that this orientation dependence is correctly given by the Cox model although its inherent stress transfer mechanism does not seem to be valid. If θ is the angle between the external tensile stress and the orientation of a fibre segment, elongation of the segment is proportional to $\cos^2\theta$, and its shear and bending are proportional to $\sin\theta\cos\theta$.

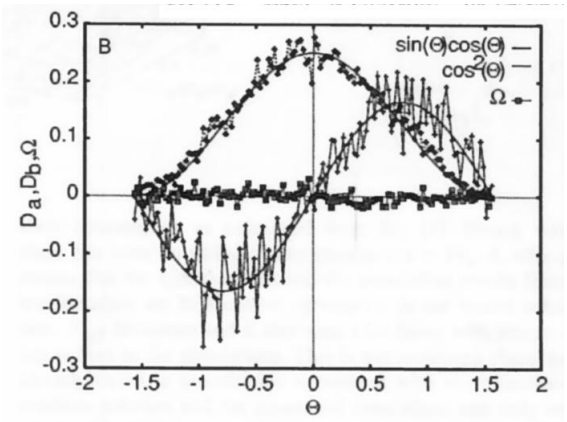

Figure 3.6. The average orientation distributions of displacements compared with the Cox model displacement fields. Bending $(\sin(\theta)\cos(\theta))$, axial $(\cos^2(\theta))$, and rotational $(\Omega(\theta))$ deformations as functions of the orientation angle θ [50].

As mentioned above, we also need the segment length distribution, which is the same as in Sec. 2.2, but now with a dilution factor a. As the arguments used above apply in 2d networks, we essentially consider a 2d projection of the real 3d fibre mat, for which a fraction (a) of the apparent crossings are not

bonded. Now the segment length distribution is given by Eq. (2.1),

$$\sigma(l) = \frac{2aq}{\pi L_f} \exp\left(-\frac{2aq}{\pi L_f} l\right), \tag{3.10}$$

and the average segment length can be written as $\hat{\ell} \equiv \pi L_f/(2aq)$. The validity of our assumption that the 2d projection of a 3d fiber mat gives the correct segment-length distribution is tested in Fig 3.7, where the comparison between Eq. (3.10) and the numerical segment-length distributions of the simulated random fibre network for parameter values $q = 4q_c$ and $q = 6q_c$ is shown.

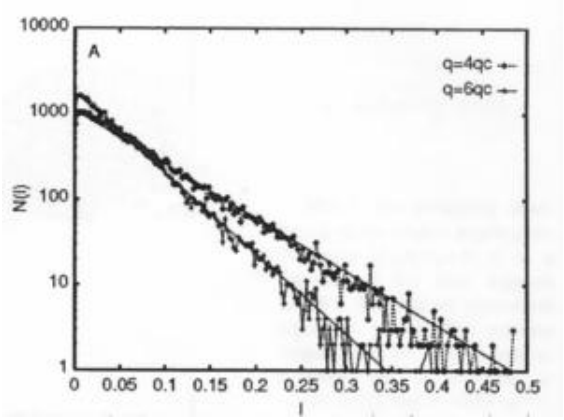

Figure 3.7. The segment-length distributions for $q/q_c = 4$ and $q/q_c = 6$ (points) in comparison with unnormalized Eq. (3.10) (straight lines) [50].

To get the elastic energy of the whole network, we must sum up all the energies of the different deformation modes. The energies are calculated by multiplying the energy of a single-segment deformation by the average number of such segments, and then integrating over the segment length distribution with appropriate limits. We also have to integrate over the angular distribution which is the same as in the shear-lag model. The elastic energy of the whole network is then given by

$$\begin{aligned} W = &\frac{Ew^2}{2}\epsilon_x^2 q \frac{L_x L_y}{L_f} \int_{-\frac{\pi}{2}}^{\frac{\pi}{2}} \frac{\cos^4\theta}{\pi} d\theta \int_0^{\ell_c} \frac{\ell}{\hat{\ell}^2} e^{-\ell/\hat{\ell}} dl \\ &+ \frac{Gw^2}{2}\epsilon_x^2 q \frac{L_x L_y}{L_f} \int_{-\frac{\pi}{2}}^{\frac{\pi}{2}} \frac{\cos^2\theta \sin^2\theta}{\pi} d\theta \int_0^{\ell_c} \frac{\ell}{\hat{\ell}^2} e^{-\ell/\hat{\ell}} dl \\ &+ \frac{Ew^4}{2}\epsilon_x^2 q \frac{L_x L_y}{L_f} \int_{-\frac{\pi}{2}}^{\frac{\pi}{2}} \frac{\cos^2\theta \sin^2\theta}{\pi} d\theta \int_{\ell_c}^{\infty} \frac{1}{\hat{\ell}^2 \ell} e^{-\ell/\hat{\ell}} dl, \end{aligned} \tag{3.11}$$

where the energies of deformations by stretching, shearing and bending are represented by the first, the second and the third term on the right hand side,

respectively, and $G = E/(2(1+\sigma))$. The last integral is an Exponential-Integral function and thus it cannot be expressed with elementary functions. Here it is best to approximate the Exponential-Integral function by a rational approximation [1],

$$E_1(z) = \frac{z^2 + a_1 z + a_2}{z^2 + b_1 z + b_2}\frac{e^{-z}}{z} + \varepsilon(z)\frac{e^{-z}}{z}, \tag{3.12}$$

where $a_1 = 2.3347$, $a_2 = 0.2506$, $b_1 = 3.3307$, $b_2 = 1.6815$ and $|\varepsilon(z)| < 5\times10^{-5}$.

On the other hand, the energy of the network can be written in the form $W = \frac{1}{2}E_e\epsilon_x^2 L_x L_y$, if it is treated as a homogeneous plate. In this way we can get an expression for the stiffness of the network as a function of w and q. The result is an effective Young's modulus (E_e) which can, after solving the other integrals in Eq. (3.11), be written in the form

$$E_e = \frac{Ew^2 q}{8L_f}\left[\left(\frac{2aqw}{\pi L_f}\right)^2 E_1(z) + \left(3 + \frac{1}{2(1+\sigma)}\right)\left[1 - e^{-z}(z+1)\right]\right], \tag{3.13}$$

where $E_1(z)$ is an Exponential-Integral (Eq. (3.12)) and parameter z equals $2aql_c/(\pi L_f)$.

We also have to take into account that not all of the segments carry load, especially near the critical percolation density. The simplest possible tranformation from q to the density of load carrying fibres q_l is given by $q/q_c = q/q_l + 0.55 + 0.45/(q_l/q_c + 1)$. This equation is just a crossover from $q = q_c$, when $q_l = 0$, to $q_l \to q - 0.55q_c$ in the limit when q_l and q both approach infinity. Thus the q in Eq. (3.13) should be replaced by q_l,

$$q_l = \frac{q_c}{2}\left\{\frac{q}{q_c} - 1.55 + \left[\left(1.55 - \frac{q}{q_c}\right)^2 - 4\left(1 - \frac{q}{q_c}\right)\right]^{1/2}\right\}. \tag{3.14}$$

A three-dimensional mat has almost the same stiffness as a two-dimensional one, provided the degree of bonding is the same and the external presssure is low enough for the fibres to bend only little [52]. We expect that the fraction of all the fibre-fibre crossings in the two-dimensional projection of a three-dimensional mat that form real contacts, behaves as $a \propto 1/q$ for large q. This is a consequence of the fact that the total number of bonds in the two-dimensional projection increases proportional to q^2, but in the three-dimensional mat new bonds are only formed at the surface of the mat. The number of contacts in the 3d mat grows therefore proportional to q. Also, if the ratio $w/(w_0 \sin\phi)$, where w is the width and w_0 is a typical segment length (see Fig. 3.2) and ϕ is the bending angle of a fibre, remains constant, only the length scale in the thickness direction of the mat is changed. Hence a remains unchanged and must be given by $a = f(w/(w_0 \sin\phi))/q$ for large q. The number

of contacts per fibre (n) is thus related to this function f such that

$$n = \frac{2}{\pi} f(w/(w_0 \sin\phi)). \tag{3.15}$$

Using Eq. (3.14) and function f, we can write Eq. (3.13) in the form

$$E_e = \frac{E w^2 q_l}{8 L_f}\left[\left(\frac{zw}{l_c}\right)^2 E_1(z) + \left(3 + \frac{1}{2(1+\sigma)}\right)\left[1 - e^{-z}(z+1)\right]\right], \tag{3.16}$$

where the function $f(w/(w_0 \sin\phi))$ appears through parameter $z \equiv 2 f l_c/(\pi L_f)$. Simulations reveal that the model gives correct results for the stiffness of mats under low external pressure provided the fibre density is $q > 3q_c$, and the fraction of bonded contacts $\alpha \geq 0.25$. Within these limits Eq. (3.16) gives the same mat stiffness as the numerical simulation as demonstrated in Fig. 3.8.

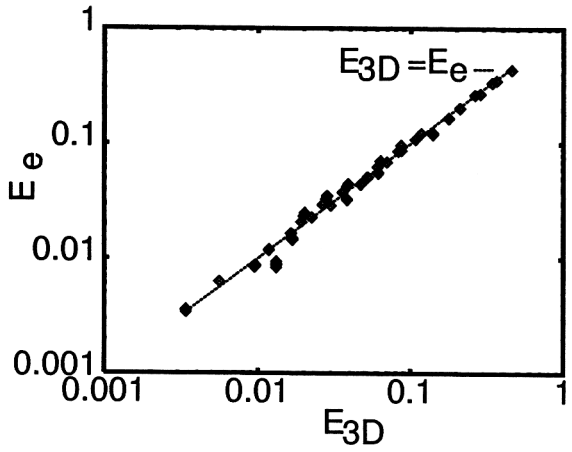

Figure 3.8. The effective-medium stiffness E_e (Eq. (3.16)) vs. the 3d simulated stiffness. Parameter values in the simulations vary in the intervals $q/q_c = 4-6$, $w = 0.003 - 0.01$, and $\theta = 0.03 - 0.11$.

Summarizing, we have found an expression for the effective Young's modulus of a random fibre network, which depends on the properties and number of its constituents together with the function f which defines the connectivity. The possibility of applying Cosserat elasticity can be neglected because the rotational deformation Ω equals zero as shown in Fig. 3.6. Because the mat has an effective response to a macroscopic deformation, when treated as a continuum plate, we can derive expressions for the other elastic constants by using continuum elasticity theory (see next).

Back to continuum theory

In order to find expressions for the other elastic constants we need to resort to continuum elasticity theory of solids [23]. That is, above a certain density we expect the mat to act as a continuum plate of in-plane dimensions L_x and L_y and thickness L_z. The coordinate system is chosen such that the z direction is normal to the plane of the mat, the y direction is along the periodic in-plane direction and the x direction is from the left to the right boundary.
The spring constant in the x direction of a continuum plate for which Poisson contraction is prohibited by periodic boundary conditions in the y direction, is [24]

$$K_x = \frac{E}{(1-\sigma^2)}\frac{L_y L_z}{L_x}. \tag{3.17}$$

Here E is the Young's modulus and σ the Poisson ratio of the plate. Moving the right boundary in the y direction corresponds to a shear deformation and yields for the spring constant in the y direction [24]

$$K_y = \frac{E}{2(1+\sigma)}\frac{L_y L_z}{L_x}. \tag{3.18}$$

Solving for the Poisson ratio from Eqs. (3.17) and (3.18), we get

$$\sigma = 1 - 2\frac{K_y}{K_x}. \tag{3.19}$$

The spring constants K_x and K_y can be easily determined for the numerical model of randomly deposited fibres. We show in Fig. 3.9 results of K_x/K_y versus fibre density for five combinations of the parameters w and ϕ. The ratio K_x/K_y clearly seems to converge to an asymptotic value $K_x/K_y \approx 3.15$, independent of the parameters even for fairly low fibre densities. This behaviour is consistent with the fibre mat behaving effectively as a continuum elastic medium. The asymptotic average ratio of K_x/K_y corresponds to a Poisson ratio of $\sigma \approx 0.37$, which is in good agreement with the typical values of σ found for paper. Based on these results we can quite confidently use continuum elasticity for $q \geq 3q_c$ and e.g., write the shear stiffness of the mat in the form

$$G_e = \frac{K_y}{K_x}E_e, \tag{3.20}$$

which, using Eq. (3.13), gives G_e in the form $G_e = G_e(q, w, \phi, \sigma, L_f, E)$.

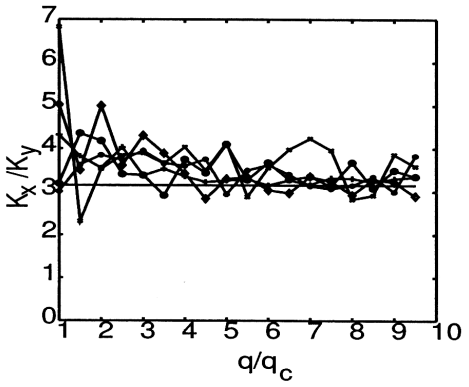

Figure 3.9. The ratio K_x/K_y for the following parameter values: $(w, \phi) = \{(0.02, 0.1), (0.04, 0.1), (0.06, 0.1), (0.02, 0.2), (0.06, 0.2)\}$. The line represents the value $K_x/K_y = 3.15$. The data is averaged over 40 samples of the size $(2.1L_f)^2$.

Chapter 4

Porosity of random fibre networks

In addition to the mechanical properties of random fibrous structures addressed in the previous chapter, they have also other important (macroscopic) parameters such as porosity.
We define here the two-dimensional (area) porosity ρ_m of a three-dimensional fibre mat as a fraction of a cross-section not covered by fibres. This area porosity divides the mat into three regions; bottom, bulk and surface region. At the bottom fibres lie flat, and the porosity is at its lowest value, while it quickly increases to a constant value in the bulk region. This behaviour can be seen in Fig. 4.1, where different lines represent different percolation densities of the mat. In the rough surface region the porosity increases from its bulk value to unity.

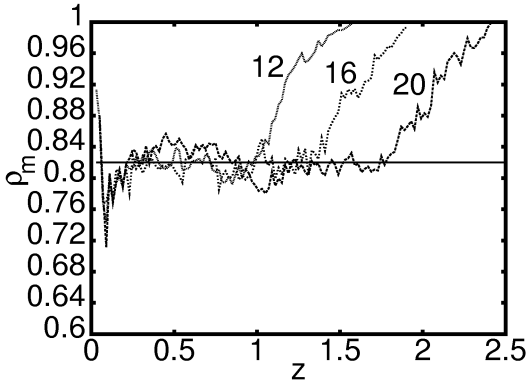

Figure 4.1. The area porosity ρ_m as a function of distance z in the thickness direction for $q/q_c = 12$, 16 and 20. The peak on the left results from fibres lying flat on the substrate, and should be discarded [49].

It should also be noticed that the density q corresponds to mass per unit area in the bulk region. The bulk density does not change when q is increased. When new fibres are deposited on the mat, they only add a new 'fibre layer' with the

same bulk density. This is seen to be true within statistical variations, as expected. Because of the surface effects, in the analysis of porosity of fibre mats, rather thick mats (i.e. large density q) should be used. As the area porosity ρ_m is constant through the bulk region of the material, it coincides there with the three dimensional porosity of the mat. Also, since the deposition process lays the fibres always at angle ϕ with respect to the plane of the mat, $1-\rho_m$ should be equal to $w^2/(L^2 \sin\phi)$, which is the area fraction in a cross section of size L^2 covered by a crossing fibre multiplied by the total number of fibre segments crossing the cross section.

The thickness of the mat can be scaled by the parameters w and $\sin\phi$ while keeping the ratio $w/(w_0 \sin\phi)$ constant. This scaling is equivalent to a scale transformation in the thickness direction of the mat, and w_0 is the typical segment length. Therefore, the area (and bulk) porosity can be expected to have the form

$$\rho_m = 1 - g\left(\frac{w}{w_o \sin\phi}\right)\frac{w^2}{\sin\phi}, \tag{4.1}$$

in which $g(x)$ is some scaling function which describes the number of segments going through a unit cross section in a plane. As explained in Ch. 3, fibres form zig-zag patterns between contacts because of the deposition rules applied. The ratio of the width (w) and the height of the zig-zagging pattern of the fibre $(w_0 \sin\phi)$ (as schematically described in Fig. 3.2) determines how many times, on the average, such bending fibre crosses the plane. Therefore, the width of a fibre can be seen as a measure for the thickness of a fibre layer in the mat, and so the ratio $(w_0 \sin\phi/w)$ determines the number the layers which one fibre covers in the structure of a fibre mat. This means that we would expect the function $xg(x)$ to act the same way as $f(x)$ defined in Sec. 3.2.2.

The bulk porosity of a mat has been determined for a number of values of $w^2/(w_0 \sin\phi)$ so that function g can be solved numerically through Eq. (4.1). The other scaling function f can be determined numerically through Eq. (3.15) from $n = (2/\pi)f(w/(w_0 \sin\phi))$. Numerical results for $f(w/(w_0 \sin\phi))$ and $\frac{w}{w_0 \sin\phi} g(w/(w_0 \sin\phi))$ are shown in Fig. 4.2.

It is evident from Fig. 4.2 that $f(x)$ and $xg(x)$ are, as expected, very similar. This similarity suggests that they should in fact coincide upon rescaling of both axis:

$$xg(x) = c_1 f(c_2 x), \tag{4.2}$$

where c_1 and c_2 are scaling constants. We show in Fig. 4.3 that by using c_1 and c_2 as fitting parameters, the two functions can indeed be made to exactly overlap with the scaling parameters $c_1 = 4.7$ and $c_2 = 0.65$. It is also worth noticing that, through function f and Eqs. (3.10), (3.13), (3.15), (3.20), (4.1) and (4.2), it seems possible to determine the entire structure and mechanical behaviour of a random beam network.

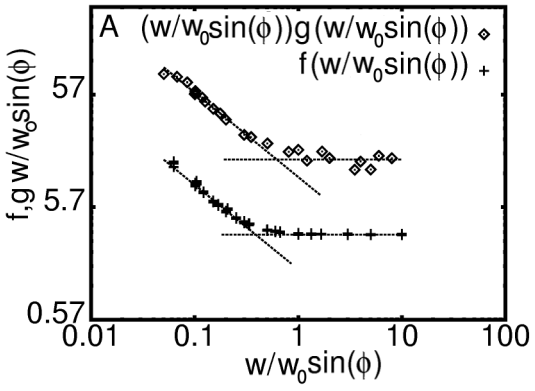

Figure 4.2. Plots of the functions $f(w/w_0 \sin\phi)$ and $(w/w_0 \sin\phi)g(w/w_0 \sin\phi)$ in a log-log scale. For small $w/w_0 \sin\phi$, the power-law $(w/w_0 \sin\phi)^{-3/4}$ is fitted to the data. For large $w/w_0 \sin\phi$ the power-law changes to a constant value with a crossover approximately at $w/w_0 \sin\phi \simeq 0.3$.

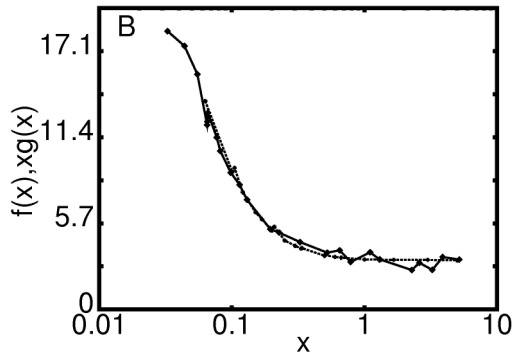

Figure 4.3. The same functions as in Fig. 4.2 in a semilogarithmic scale with the function $xg(x)$ rescaled according to Eq. (4.2) with $c_1 = 4.7$ and $c_2 = 0.65$. The scale on the y axis is given by $q_c \approx 5.7$.

The form of function f suggests a power-law dependence for small values of the argument, and it clearly levels off to a constant at large values of the argument (n approaches its minimum average value $n = 2$). Simple least-squares fitting in the two respective regimes gives

$$\begin{cases} f(x) \propto x^{-\frac{3}{4}}, & x \lesssim 0.3 \\ f(x) = \text{const.}, & x \gtrsim 0.3 \end{cases} . \tag{4.3}$$

For the sake of completeness it should be mentioned that it would also be possible to study the porosity of a two-dimensional fibre mat by letting the thickness of the fibres in a three-dimensional mat vanish. The porosity of such a material will decrease continuously to zero when the number of constituents

is increased, and its behaviour will thus be qualitatively different from that of a three-dimensional mat. For this reason two-dimensional fibre mats are not considered here.

We have demonstrated above that the porosity of a random fibre mat is determined by parameters related to the properties of the constituents together with essentially the same measure of connectivity as the one applicable to its elastic properties. It should be noticed that a sedimented material is defined by its constituents *and* the specific deposition process (see Sec 3.1), which together define the texture of the material. Sedimented materials with similar constituents but created by different processes do not usually have the same relations between their porosity and stiffness on the one hand, and connectivity on the other hand. Therefore the function that describes the connectivity must be process dependent, which justifies the term 'process function' for function f. We have only considered random fibre mats here, but similar approach can be used for other kinds of randomly 'deposited' materials. For random packings of elastic (two- or three-dimensional) discs, e.g., this process function is the trace of the average fabric tensor $\langle n \rangle$ [49].

Chapter 5

Stiffness evolution in random fibre networks

In this chapter we present a model for stiffness evolution in a 2d random fibre network. In this model evolution is realised by moving fibre material from one location to another based on local load. The topology of the network is not changed although it can be argued that changing the topology (i.e. shape) is more favourable than changing the material properties [43]. For example, the basic bone development is determined by genes, but the final structure is governed by adaptive response to mechanical load. In 1892, J. Wolff [46] postulated that the form of bone is related to mechanical stress by a mathematical law. In his law, Wolff referred to form and function as a *static* mathematical relationship between trabecular architecture and stress trajectories, and he believed that the shape of the bone is inherited. Regardless of these misconceptions, his law has been accepted as a foundation for the functional adaptation of bone [9].
Previous simulation results [15] have also confirmed the results we have found that Wolff's law is very general, and strengthening of a structure in the direction of an external principal load can be achieved using very simple rules. We also give an estimate on how effective this strenghtening procedure is for fibre networks.

5.1 Introduction

The adaptivness of the mammal skeleton is a well documented phenomenon. The skeleton of astronauts, for example, becomes weaker the more time they spend in a gravity-free environment. This is due to lack of mechanical loading of the bones. On the other hand, athletes usually develop anomalous bone strength due to large amounts of spezialized training. A tennis player e.g. develops a stronger bone structure in the arm with which he holds the racket. The

basic mechanism behind this remodelling of bones is the activity of two types of cells: osteoblasts which form new bone and osteoclasts which devour bone. The rate of remodelling and devouring depends obviously on the amount of mechanical loading.
Understanding this phenomenon, and the increased bone loss in elderly people (osteoporosis), which is related to it, is of course important, and it has received wide interest in the medical research [15]. To understand this phenomenon from a statistical physics point of view has, to our knowledge, not been attempted so far. The question we address here is: How efficiently can nature optimize the strength-to-weight ratio of a random structure by strengthening parts which are much loaded and devouring parts which experience little load?

5.2 Numerical model

In order to investigate the physics of this type of strength adaptivness, we introduce a minimal model of a network of randomly deposited elastic fibres. The total mass of the network is set to be constant. The mechanical load on each fibre segment due to the applied global loading conditions can be calculated repeatedly by solving a set of linear equations. After each time the elastic equilibrium is determined, some mass is transferred from the least to the most loaded fibre segment. This way the load distribution and the stiffness of the network is changed continuously.

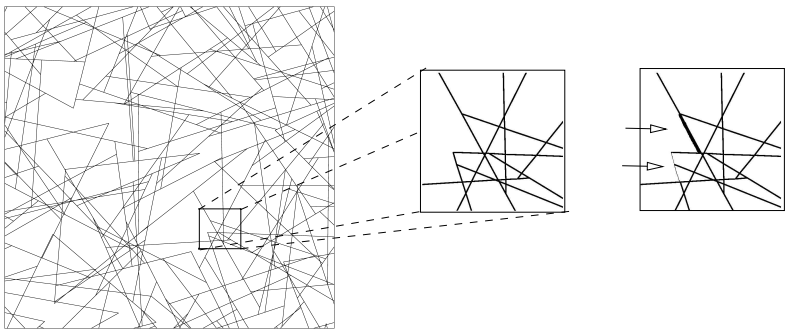

Figure 5.1. A 2d random fibre network with parameters $q = 4q_c$ and $L_f = 1$ in an area of 2.1×2.1, and an enlarged part of it for the visualization of mass transfer. Topology of the network is conserved in the mass transfer, only the widths of the two segments are changed. Arrows indicate the segments between which mass transfer takes place.

In practice this means that in the beginning we strip away all dangling ends of the fibres and save the corresponding amount of mass for later use (in order to conserve the total mass of the system). The removal of the dangling ends can be done, as they do not contribute to the global stiffness of the network. It

is done in order to reduce the number of nodes and to minimize the needed computational task.

Further, after solving the deformation of each fibre segment, as a response to global loading with the given boundary conditions, we calculate the elastic energy of every segment. If there is still mass left from the dangling ends, we use and move it to the most energetic segment. Otherwise we take mass from the segment containing the least elastic energy and move it to the most energetic segment. The mass transfer is done in proportion to the original width of the segment. None of the segments is completely removed, only their width is changed so the topology of the network is conserved.

We have defined a relative minimum/maximum limit for the segment width to avoid unlimited shrinkage/growth of it. Otherwise this would create pathological geometries in the evolving network and we do not want to change the topology, only the mass distribution among the segments. After the mass transfer, the elastic equilibrium of the system is recalculated, and mass transfer is then repeated. Iterations are done until a predefined maximum number of iterations is reached.

The elastic energy of the whole random fibre network can be calculated from the local stresses of each segment. The elastic energy of the network is then the sum of the elastic energies of all the segments. Through loading conditions we are able to produce different kinds of deformation modes in the network. We consider here tensile stress, but could also consider in a similar fashion e.g. the cases of pure shear stress and a stress mode that consists of opposite phase sine-waves on the left and right sides of the network as shown in Fig. 5.2. Because the y direction is periodic, the elastic network can be thought to be rolled into a tube. Deformation modes can now be seen as elongation of a tube, twisting the ends of a tube in opposite directions, and bending of a tube.

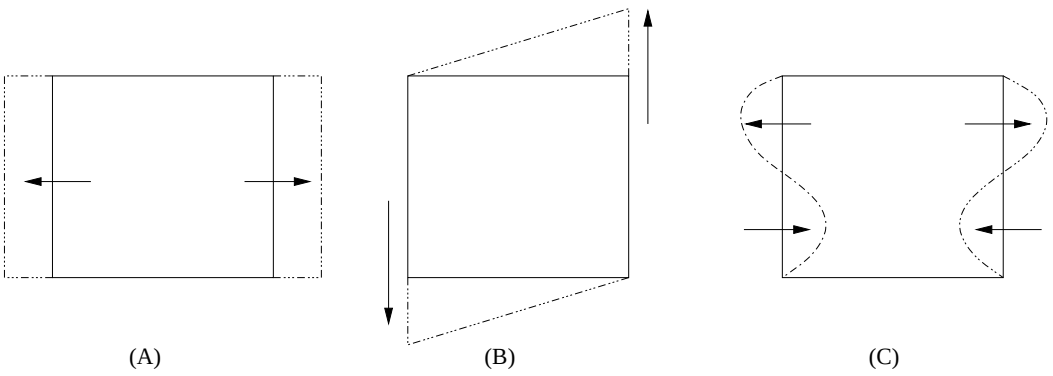

Figure 5.2. Possible types of deformation modes; tensile stress, pure shear stress and a stress mode composed of opposite-phase sine waves.

5.3 Calculation of elastic energy

In order to start modelling our network on a computer we return back to the basics of elasticity theory (see Sec. 1.2). The building blocks of our network are linear elastic rods. From Eq. (1.7) we get for the elongation of a rod in the x direction

$$u_x = \frac{l}{EA} F_x, \tag{5.1}$$

where l is the length of the rod, A is the cross-sectional area of the rod and u_x is the displacement at the other end of the rod with one end clamped, and F_x is the applied force. This is similar to a spring in the linear case, and it can be written in the form $F_x = ku_x$, where the *stiffness constant* is $k = EA/l$.

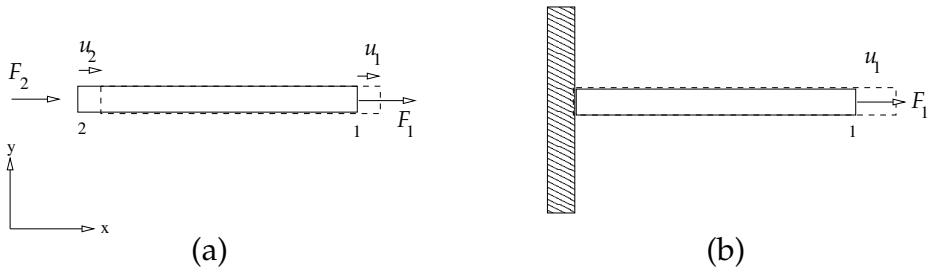

Figure 5.3. (a) Rod under loads F_1 and F_2 acting on ends 1 and 2 of the rod, respectively, and (b) rod under load F in the x direction when the movement of the other end is prohibited. Corresponding displacements u_i are also marked.

If the rod is part of a bigger structure, we have to take into account the case that both ends of the rod can move as shown in Fig. 5.3(a). We need to write down the connection between displacements u_1 and u_2 (numbers denote the ends of the rods) and their respective forces F_1 and F_2. In matrix form this can be written as

$$\begin{Bmatrix} F_1 \\ F_2 \end{Bmatrix} = \begin{bmatrix} k_{11} & k_{12} \\ k_{21} & k_{22} \end{bmatrix} \begin{Bmatrix} u_1 \\ u_2 \end{Bmatrix}, \tag{5.2}$$

or shortly as

$$\{F\} = [K] \cdot \{U\}. \tag{5.3}$$

The stiffness constants k_{ij} can now be easily calculated based on equilibrium condition fot the acting forces. Because k_{ij} represents the force at point i when the displacement u_j is set to unity, and other displacements are zero, we can solve one column at a time from the stiffness matrix. Setting $u_1 = 1$ and $u_2 = 0$ we get a situation described in Fig. 5.3 and Eq. (5.1). The force at the right end of the rod is now

$$F_1 = k \cdot 1 = k_{11}, \tag{5.4}$$

and the force at the left end is obtained from the equilibrium condition[1]

$$F_2 = -F_1 = -k \cdot 1 = k_{21}. \tag{5.5}$$

Similarly, by setting $u_1 = 0$ and $u_2 = 1$ we get

$$\begin{cases} F_2 = k \cdot 1 = k_{22} \\ F_1 = -F_2 = -k \cdot 1 = k_{12}. \end{cases} \tag{5.6}$$

The stiffness matrix in the equilibrium equation Eq. (5.3), which describes the equilibrium conditions for the nodes (end points of the rod), can now be written as a 2×2 matrix,

$$[K] = \begin{bmatrix} \frac{EA}{l} & -\frac{EA}{l} \\ -\frac{EA}{l} & \frac{EA}{l} \end{bmatrix}. \tag{5.7}$$

If we also want to take into account the other deformation modes, namely bending and rotations, we can do this separately from the elongination as there is no coupling between them. We start by defining the displacement vector U as

$$U = \{u_{1y}, u_{1\theta}, u_{2y}, u_{2\theta}\}^T, \tag{5.8}$$

where the components u_y are the displacements of the respectively numbered rod end in the y direction, and the components u_θ are the angles of rotation, respectively. Similarly, we define the corresponding force vector as

$$F = \{F_1, M_1, F_2, M_2\}^T, \tag{5.9}$$

and would like to derive the familiar equation $\{F\} = [K]\{U\}$ between them. We can now use the same method as previously for the elongination of the rod. We set each of the displacements to unity one at a time, while other displacements are zero, and calculate the forces acting on the rod. Considering the case in Fig. 5.4(a), where all degrees of freedom but u_{1y} is fixed, we get relations

$$\begin{cases} F_1 = k_{11} u_{1y} \\ M_1 = k_{21} u_{1y} \\ F_2 = k_{31} u_{1y} \\ M_2 = k_{41} u_{1y}. \end{cases} \tag{5.10}$$

We now need expressions for the displacement $u_y(x)$ and for the moment $M(x)$. We start by considering small deflections of the rod. If the radius of curvature of the bent rod is small, we arrive at a differential equation which describes the line of bending of the rod assuming that it takes place in the xy

[1] As the body does not move, the sum of the acting forces must be zero.

plane [24],

$$EI\frac{d^2u_y}{dx^2} + M(x) = 0, \tag{5.11}$$

where I is the moment of inertia of the rod and $M(x)$ is the moment inflicted at point x of the rod.

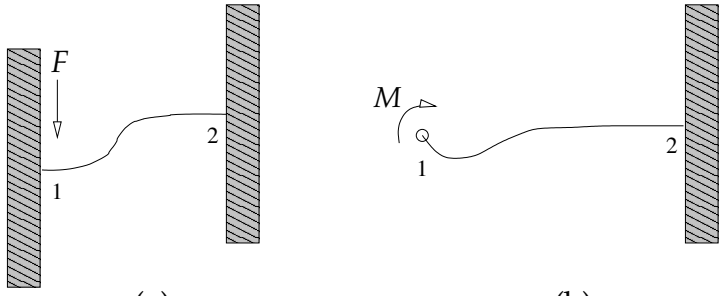

Figure 5.4. (a) Pure transverse translation of the rod with force F while the other end is clamped and (b) bending of a rod with moment M while the other end is clamped.

The moment $M(x)$ in the case of Fig. 5.4(a) is of the form

$$M(x) = \frac{F_1 l}{2} - F_1 x. \tag{5.12}$$

Combining this with the Eq. (5.11), we can write the differential equation in the form

$$EI\frac{d^2u_y}{dx^2} = -\frac{F_1 l}{2} + F_1 x. \tag{5.13}$$

Solving this with the following boundary conditions,

$$\begin{cases} u_y(0) = u_{1y} \\ u_\theta(0) = u'_y(0) = 0 \\ u_y(l) = 0 \\ u_\theta(l) = u'_y(l) = 0, \end{cases} \tag{5.14}$$

we arrive at the solution

$$u_y(x) = \frac{F_1 l^3}{12EI}\left(1 - \frac{3x^2}{l^2} + \frac{2x^3}{l^3}\right). \tag{5.15}$$

The maximum value for u_y given by Eq. (5.15) is $max(u_y) = u_{1y} = \frac{F_1 l^3}{12EI}$, which, by solving for F_1 (as the displacement u_{1y} was set to unity), gives us the first k_{11} element of the stiffness matrix as seen from Eq. (5.10). From Eq. (5.12) it can be clearly seen that the maximum of the moment is given by $max(M) = M_1 = -M_2 = Fl/2$, which gives us the stiffness matrix element

$k_{21} = M_1/u_{1y} = F_1 l/2 = 6EI/l^2$. In addition we know that

$$\begin{aligned} F_2 = -F_1 \Rightarrow k_{31} &= \frac{F_2}{u_{1y}} = -\frac{12EI}{l^3} \\ M_2 = M_1 \Rightarrow k_{41} &= \frac{M_2}{u_{1y}} = \frac{6EI}{l^2}. \end{aligned} \tag{5.16}$$

The other columns of the stiffness matrix can be determined similarly. Because of the symmetry of the stiffness matrix (first row is the same as the already determined first column) and we know that for any combination of bending and rotation we have $F_2 = -F_1$, so the elements of the third row are complements of the first row. What is left to be determined are the elements k_{22} and k_{24}, as the symmetry of the stiffness matrix determines $k_{42} = k_{24}$ and $k_{44} = k_{22}$.
To solve the remaining parts of the second column of the stiffness matrix, we consider a case where $u_{1\theta} = 1$ and $u_{1y} = u_{2y} = u_{2\theta} = 0$. This means that the following boundary conditions,

$$\begin{cases} u_y(0) = 0 \\ u_\theta(0) = u_y'(0) = u_{1\theta} \\ u_y(l) = 0 \\ u_\theta(l) = u_y'(l) = 0, \end{cases} \tag{5.17}$$

are imposed. The moment is now given by $M(x) = M_1\left(1 - \frac{3}{2l}x\right)$, and combining this with Eq. (5.11), we can the calculate solution of the attained differential equation with the boundary conditions Eq. (5.17). Remembering that we consider now only small deformations in the linear case, we have $u_\theta = \frac{du_y}{dx}$, so the only thing we need to solve is the first derivative of $u_y(x)$. The first derivative of the displacement in the y direction is

$$\frac{du_y}{dx} = \frac{M_1 l}{4EI}\left\{-\frac{3}{l^2}x^2\frac{4}{x}x + 1\right\}, \tag{5.18}$$

and we get the angle of rotation for the bending angle of the rod as $u_{1\theta} = \frac{M_1 l}{4EI}$, which defines the element k_{22} of the stiffness matrix. As we know that $M_2 = -M_1/2$, we find that the element k_{24} is equal to $2EI/l$.
Summarizing the previous calculations, we find for bending and rotations the stiffness matrix in the form

$$[K] = \begin{bmatrix} \frac{12EI}{l^3} & \frac{6EI}{l^2} & -\frac{12EI}{l^3} & \frac{6EI}{l^2} \\ \frac{6EI}{l^2} & \frac{4EI}{l} & -\frac{6EI}{l^2} & \frac{2EI}{l} \\ -\frac{12EI}{l^3} & -\frac{6EI}{l^2} & \frac{12EI}{l^3} & -\frac{6EI}{l^2} \\ \frac{6EI}{l^2} & \frac{2EI}{l} & -\frac{6EI}{l^2} & \frac{4EI}{l} \end{bmatrix}. \tag{5.19}$$

This method of getting the stiffness matrix is called the *direct method*.
Using Eqs. (5.7) and (5.19), we can write down the stiffness matrix for all cases

treated above. When the displacement vector U for a 2d beam element is written in the form $U \equiv \{u_{1x}, u_{1y}, u_{1\Omega}, u_{2x}, u_{2y}, u_{2\Omega}\}^T$, the corresponding force vector as $F \equiv \{F_{1x}, F_{1y}, M_{1\Omega}, F_{2x}, F_{2y}, M_{2\Omega}\}^T$, we assume that the fibres are rigidly bonded to each other at every fibre-fibre crossing, and the segments are presented as node-node pairs, we can express the stiffness matrix in the form

$$\mathbf{K} = \begin{pmatrix} \frac{EA}{l} & 0 & 0 & -\frac{EA}{l} & 0 & 0 \\ 0 & \frac{12EI}{l^3} & \frac{6EI}{l^2} & 0 & -\frac{12EI}{l^3} & \frac{6EI}{l^2} \\ 0 & \frac{6EI}{l^2} & \frac{4EI}{l} & 0 & -\frac{6EI}{l^2} & \frac{2EI}{l} \\ -\frac{EA}{l} & 0 & 0 & \frac{EA}{l} & 0 & 0 \\ 0 & -\frac{12EI}{l^3} & -\frac{6EI}{l^2} & 0 & \frac{12EI}{l^3} & -\frac{6EI}{l^2} \\ 0 & \frac{6EI}{l^2} & \frac{2EI}{l} & 0 & -\frac{6EI}{l^2} & \frac{4EI}{l} \end{pmatrix}. \tag{5.20}$$

The solving of the random fibre system consisting of fibre segments is started by calculating the local stiffness matrix for each 2d element. As concluded above, the matrix Eq. (5.20) defines the interaction between two connected bonds where the Young's modulus of a fibre segment is E, the length is l, the moment of inertia is I, and the cross-sectional area is A. We have considered fibres with square cross section of area $A = w^2$, so that the moment of inertia is $I = w^4/12$. The stiffness matrix is valid only for values $w \ll l$. For shorter segments the bending stiffness Ew^4/l^3 should be replaced by the shear modulus $Ew^2/(2(1+\sigma)l)$, at least in the first approximation.

After creating all the local stiffness matrices, they need to be rotated to the same coordinate system before constructing the global stiffness matrix. This must be done also for the force and displacement vectors. The global stiffness matrix is created by summing up all the degrees of freedom corresponding to the same nodes. Formally this means that the elements a_{ij} of the global stiffness matrix are obtained as a sum of the elements of the corresponding local stiffness matrices. The degrees of freedom in each node are to be globally numbered, and the elements of the different local stiffness matrices that refer to the same node, can be summed.

The procedure is similar in three dimensions; only the number of degrees of freedom is increased so that the local stiffness matrix becomes a 12×12 matrix (six degrees of freedom per node).

In this way we construct a linear system of equations,

$$A\mathbf{x} = \mathbf{b}, \tag{5.21}$$

where A is the global stiffness matrix, the entries in the deformation vector ($\mathbf{x}$) correspond to the degrees of freedom of each node, and the entries in the force vector ($\mathbf{b}$) to the forces acting upon them.

Solving the linear system

Systems like Eq. (5.21) can solved by using direct solvers (usually based on Gaussian elimination) or iterative methods. The convenience of using iterative methods comes from the facts that i) the initial values can be approximated beforehand, and ii) in iterative methods we can define the desired accuracy of the solution [11].
It can be shown that matrix A in Eq. (5.21) is *symmetric* and *positive-definitive*. We can then represent this equation as a minimatization problem of a quadratic functional (many efficient iterative methods have been derived for optimization problems) [17,47,44]

$$J(\mathbf{x}) = \frac{1}{2}\langle A\mathbf{x}, \mathbf{x}\rangle + \langle \mathbf{b}, \mathbf{x}\rangle, \tag{5.22}$$

where $\langle \cdot, \cdot \rangle$ is the usual Euclidean inner product in $\mathbb{R}^n$. The minimum of the function J is given by the condition $\nabla J = 0$. Thus, by minimizing the function J, we can solve the initial linear system Eq. (5.21). Given an initial approximation $\mathbf{x}_0 \in \mathbb{R}^n$ of the exact solution $\mathbf{x}$, our task is to find successive approximations $\mathbf{x}_k \in \mathbb{R}^n$,

$$\mathbf{x}_{k+1} = \mathbf{x}_k + \alpha_k \mathbf{d}_k; \quad k = 0, 1, \ldots, \tag{5.23}$$

where $\alpha_k > 0$ is the step size and $\mathbf{d}_k \in \mathbb{R}^n$ are the search directions. Iterative methods differ in their choice for the step size and search direction. We have used a conjugate gradient method in which we select the optimization directions $\mathbf{d}_k$ so that they are conjugated to A, e.g.,

$$\langle d^{(i)}, A d^j \rangle = 0, \qquad \forall i \neq j. \tag{5.24}$$

Faster convergence of iterative methods can be achieved by using an appropriate preconditioner. A preconditioner maps the original problem to a different system,

$$\bar{A}\bar{x} = \bar{b}, \tag{5.25}$$

which hopefully exhibits better convergence characteristics. An unsuitable preconditioner, or no preconditioning at all, may result in a very slow rate or lack of convergence. Preconditioning matrices M for symmetric linear systems, as the one we consider here, are typically based on incomplete factorizations. The method used is called incomplete Cholesky factorization in which the preconditioning matrix is of the form

$$M = PLDL^T P^T = A - R, \tag{5.26}$$

where P is a permutation matrix, L is a lower triangular matrix with unit diagonal elements, D is a diagonal matrix and R is a remainder matrix.

In our work we used commercially available NAG-library subroutines. The F11JAF, which stands for black-box Incomplete Cholesky factorization preconditioner, and F11JCF, which is a conjugate gradient solver [31], were used to solve the linear system of Eq. (5.21).

Shortest path

A simple Floyd's (Floyd 1962) algorithm is used to compare the emerging 1d-structures, the 'elastic paths', with the geometrically shortest distance across the mat. The algorithm has been modified so as to give also the actual path in addition to just calculating the length of the path [2, 3]. Floyd's algorithm is of order $O(n^3)$, but is used because of its ease of use in comparison with Dijkstra's algorithm, because the networks are not very large, and the distances are to be calculated just once. Details of the algorithm used are given in Appendix A.

5.4 A simple analytical model

Our model is based on the assumption that the previously described process will create an 'elastic path' which the process tends to strengthen. Its maximum strength is determined by the shape of the assumed structure, which would best resist the applied stress.
We limit the mass of one segment to be at most 500% from its original value. This way we also expect to see an upper bound for the value of the effective stiffness in the direction of the applied stress. This limit can be calculated by considering a single long segment with length L_x, cross-sectional area $5w^2$ and Young's modulus E, which extends from the left side to the right side of the system. This one segment gives the maximum value for the *effective* Young's modulus. For the applied mass transfer constant we get a simple linear equation for the change of network modulus (E_n) in terms of iteration steps,

$$E_n(t) = \frac{a\hat{\ell}w^2}{L^2}\left(E - \frac{E_e}{q}\right)t + E_e, \tag{5.27}$$

where E_e is an effective Young's modulus (same as in Eq. (3.13)), E is the Young's modulus of one segment and is usually set to $E = 1$, L is the linear system size, a is a mass transfer constant, $\hat{\ell}$ is the average segment length (same as in Eq. (2.1)), w is the width of the fibres, t is the iteration step parameter, and q is the density of the network.
In the case of tensile stress, the assumed shape is a single segment which extends through the system in the direction of the applied stress. For pure shear, we would expect formation of two crossing straight paths; one from the upper

left corner to the lower right corner and the other from the upper right corner to the lower left corner. For pure shear E_e should be replaced by Eq. (3.20), and L by $\sqrt{2}L$ (assuming $L_x = L_y \equiv L$). In the case of bending, two 'elastic' paths should be formed at the locations of minimum and maximum strain. The theory could be improved by replacing the system size L by an estimate of the length of the geometrically shortest paths.

5.5 Results

We have simulated stiffness evolution in a 2d random fibre network with the rules described above [22]. For applied tensile tensile stress the process creates a structure shown in Fig. 5.5 as the final result of the iteration process. In this figure the thicker lines mark the strengthened parts of the fibre network, and the geometrically shortest path is marked with a thick dash line on the side of the path (notice the periodic boundary conditions in the vertical direction).

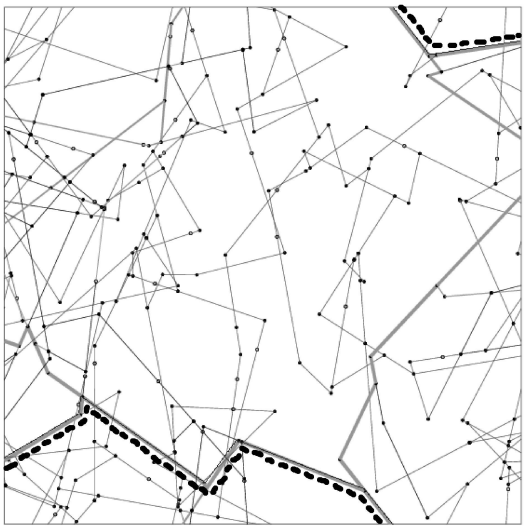

Figure 5.5. Result of the applied evolution process under tensile stress after 10000 iterations. At this low density $q = 2q_c$ the formed 'elastic path' shown by the thick line follows closely the geometrically shortest path *(thick dash line)*, but creates also some bifurcations. Dots denote the contact nodes of the segments.

To understand the effects that our iteration process creates in the structure and in the stiffness properties of the network, we start by looking at a few statistical properties. First we look at the concentration of the relative elastic energy in different parts of the network as the evolution process is iterated.
By following the relative elastic energy content (see Fig. 5.6) of thinner and thicker segments, and the elastic energy of the segments which do not change their width, we see that as the iteration process proceeds, the strengthened

'path' begins to contain more and more of the total elastic energy. The effective Young's modulus of the fibre network saturates to its maximum value at the same time as the relative elastic energy of the thicker segments approaches unity. At the same time also the segments whose width stays the same, start to carry some of the relative elastic energy.

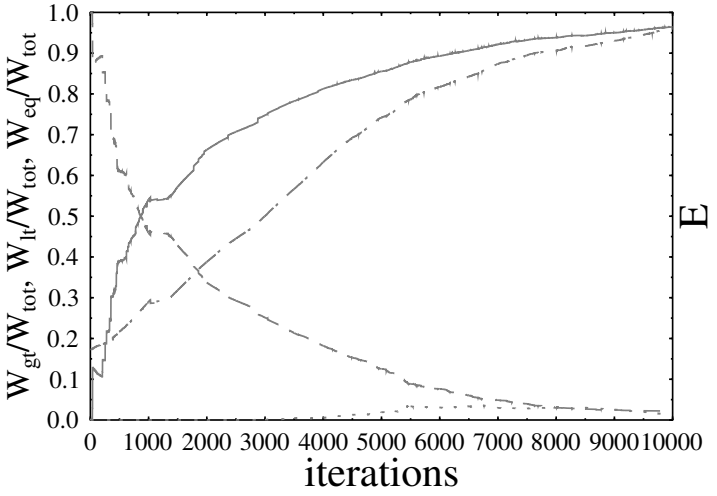

Figure 5.6. The relative elastic energy of strengthened segments *(full line)*, elastic energy of segments from which mass has been taken off *(dashed line)*, and the elastic energy of segments whose width stays the same through the iteration process *(dotted line)*. The effective Young's modulus *(dashed-dotted line)* saturates at the same time as the strengthened structure begins to contain essentially the whole elastic energy, i.e., its relative proportion of the total elastic energy approaches unity.

This means that the strengthened parts of the random fibre network begin to contain essentially the whole elastic energy of the network. This behaviour is not generally true. For example, at high fibre densities the relative elastic energy of the strengthened fibres never reaches unity because it would mean a change in the topology of the network, which is not allowed. The fact is though that the effective Young's modulus and the relative elastic energy of the thick segments in the network saturate at the same time.

Next we analyse the stress-transfer mechanisms, and study the evolution of the stress distribution during the process. The normalised strain distribution can be divided into two different distributions as described in Sec. 3.2, and the whole distribution is given by Eq. (3.3). From Fig. 5.7 we can qualitatively see how the distribution evolves in the process. During the iteration the load bearing strain distribution moves towards higher strain, and the compressive deformation distribution narrows down. This means that the contribution of

compressive forces to the total elasticity of the network reduces during the iteration process.

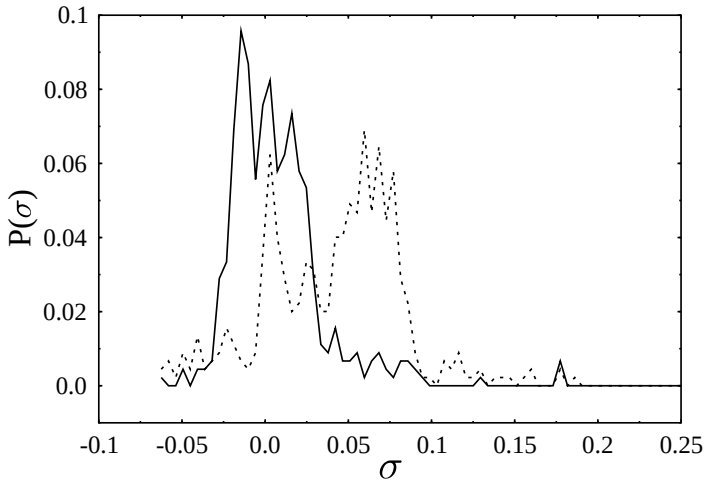

Figure 5.7. Evolution of the normalised strain distribution in a random fibre network under tensile stress for $L_f/w = 16.67$, $q = 2q_c$. Distribution is shown after 1 *(solid line)* and 9800 *(dashed line)* iteration steps.

Finally, we show our main result in Fig. 5.8. In this figure we show simulation results for the time evolution of the Young's modulus of a network under tensile stress as a function of iteration steps for nine different runs. At first the elastic modulus of the whole network grows fast (linearly), but saturates then due to the fact that there is no more mass to transfer unless the topology of the network would be changed. In the saturated regime the mass transfer takes place between such fibres which do not change the stiffness of the network. Also shown in this figure are the upper limits imposed by our simple theory. The first upper limit is due to Eq. (5.27), and the upper limit in the saturation area is due to our naïve assumption that the assumed shape of the strengthened structure is a single segment which extends through the system in the direction of the applied stress as discussed in Sec. 5.4.

The high variation in the results is due to high variation in the structure of the network at low fibre densities. For higher fibre densities the emerging structure becomes less localised. The behaviour for increasing fibre density is at least partly due to the increase of the width over length ratio of the fibre segments, i.e., the amount of short segments increases in the network as more and more fibres are added to the network. These results show that our model is to some extent capable of predicting the effect of this type of evolution process on random fibre networks.

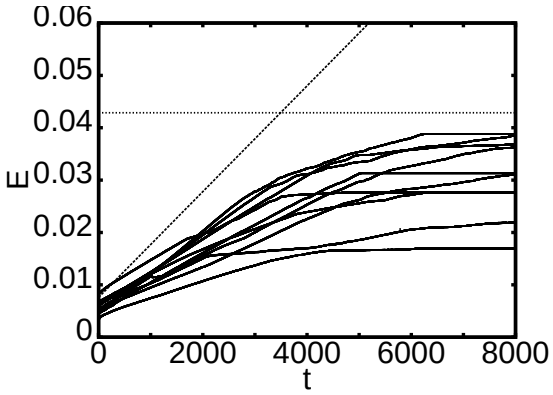

Figure 5.8. Dotted lines are the theoretical upper limits discussed in the text. Simulation results for the Young's modulus of a network under tensile stress, for $q = 2q_c$, $w = 0.02$, $L_f = 1.0$ and $a = 0.09$, are shown with full lines.

5.5.1 Tests on 3d random fibre network

We have also done some preliminary tests with 3d networks and the main assumption, that there emerges an elastic path, seems to hold at low densities. For higher densities the elastic path bifurcates and becomes fragmented. This may be due to high concentration of short fibres tangential to the external load, which creates a large amount of singular geometries, and our assumption of linear elastic fibres does not hold anymore. There is also indication of an almost exponential growth (see Fig. 5.9) in the effective Young's modulus at the beginning of the iterations, and thus our linear prediction (Eq. (5.27)) seems not to hold in this case, but these results are only preliminary and need to be confirmed.

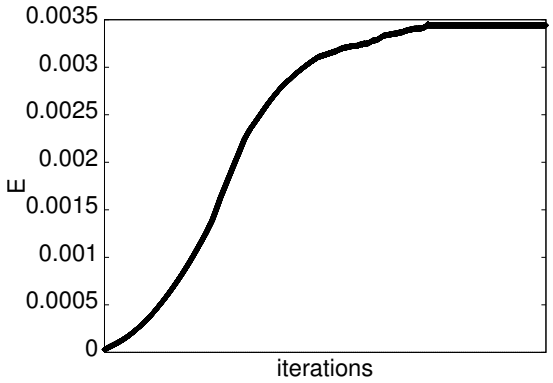

Figure 5.9. Evolution of the effective Young's modulus in a 3d random fibre network.

Chapter 6

Conclusions and Discussion

As random fibre networks offer a good strength over weight ratio in addition to a relatively easy manufacturing process, the understanding of these materials is important from an application as well as an academic point of view. Materials of this kind include human bone, glass-fibre felts and paper. An important question, e.g., is how to change the properties of constituents in order to get a desired property in the material as a whole.
A new mean field theory for the elasticity of random two dimensional networks of fibres has been developed [50], which for a fairly wide range of parameters agrees very well with the results of direct numerical simulations. An essential feature in this theory is the connectivity of the network, i.e., the average number of contacts per fibre, which together with the properties of individual fibres completely determines the elasticity, and also the porosity [3], of the network. The theory has been generalised [52] to three dimensions by determining numerically the ratio of apparent contacts which appear in the two dimensional projection of the three dimensional structure. Also in this case agreement with direct numerical simulations was found to be very good. Extension to other disordered structures, e.g. granular packings, of the theory is possible [49].
Organic materials are built up by evolution to be suitable for their job. This does not mean that nature makes some kind of optimisation. Evolution which builds up a structure is due to a process which creates alteration (adaptation) and those alterations which are beneficial will continue [43]. This process is also called *natural selection*. In the end, the information about the structure is not enough for us to understand its properties. We also need to know the underlying mechanisms involved to know how the structure is formed and how they interact. This way even a simplistic model for the stiffness evolution of random fibre structures could shed some light into this process.
Here we considered 'stiffness evolution' in two dimensional networks of elastic fibres. As a first attempt, the evolution strategy was chosen such that mass is moved from the least loaded segment to the most loaded one, and the pro-

cess is then iterated. This way the mass of the network stays the same. Evolution of stress bearing structures is then followed under a constant strain. A second possibility could be to use strain instead of loading.
At first the elastic modulus of the whole network grows fast but saturates then due to the fact that there is no more mass to transfer. In the saturated regime the mass transfer takes place between such fibres which do not change the stiffness of the network.
We found e.g. that for low density networks, the developing stress bearing structure becomes localised around a single path for applied tensile stress, while the structure becomes less localised for increasing density of the network. This behaviour for increasing q is at least partly due to the increasing width over length ratio of the fibre segments with increasing density. In low density networks the main part of the stress bearing structure is also geometrically the shortest path across the network.

Bibliography

[1] ABRAMOWITZ, M. AND STEGUN, I. (eds.), *Handbook of Mathematical Functions* (Dover, 1972).

[2] AHO, A., HOPCROFT, J., AND ULLMAN, J., *The design and analysis of computer alghorithms*, Addison-Wesley series in computer science and information processing (Addison-Wesley, 1974).

[3] CORMEN, T., LEISERSON, C., AND RIVEST, R., *Introduction to algorithms*, The MIT electrical engineering and computer science series (The MIT Press, 1990).

[4] COX, H., *The elasticity and strength of paper and other fibrous materials*. Brit. J. Appl. Phys. **3** (1952) 72–79.

[5] DENG, M. AND DODSON, C., *Paper, An engineered Stochastic structure* (Tappi Press, 1994).

[6] DUXBURY, P., BEALE, P., AND LEATH, P., *Size effects of electrical breakdown in quenched random media*. Phys. Rev. Lett. **57** (1986) 1052–1055.

[7] DUXBURY, P., BEALE, P., AND LEATH, P., *Errata: Size effects of electrical breakdown in quenched random media*. Phys. Rev. Lett. **59** (1987) 155.

[8] FENG, S. AND SEN, P., *Percolation on elastic networks: New exponent and threshold*. Phys. Rev. Lett. **52** (1984) 216–219.

[9] FORWOOD, M. AND TURNER, C., *Skeletal adaptions to mechanical usage: Results from tibial loading studies in rats*. Bone **17 (4(Suppl))** (1995) 197s–205s.

[10] DE GENNES, P., *On a relation between percolation theory and the elasticity of gels*. J. Phys, Lett. (1976) L–1.

[11] HAATAJA, J., HEIKONEN, J., LEINO, Y., RAHOLA, J., RUOKOLAINEN, J., AND SAVOLAINEN, V., *Numeeriset menetelmät käytännössä (in finnish)* (CSC-Tieteellinen laskenta Oy, 1999).

[12] HELLÉN, E., ALAVA, M., AND NISKANEN, K., *Porous structure of thick fiber webs*. J. Appl. Phys. **81** (1997) 6425–6431.

[13] HENDRICKSON, B., *Conditions for unique graph realizations*. SIAM J. Comput. **21** (1992) 65–84.

[14] HERRMANN, H. AND ROUX, S. (eds.), *Statistical models for the fracture of disordered media*, Random materials and processes (North-Holland, 1990).

[15] HUISKES, R., RUIMERMAN, R., VAN LENTHE, G., AND JANSSEN, J., *Effects of mechanical forces on maintenance and adaptation of in trabecular bone*. Nature **405** (2000) 704–706.

[16] JACOBS, D. AND THORPE, M., *Generic rigidity percolation: The pebble game*. Phys. Rev. Lett. **75** (1995) 4051–4054.

[17] JOHNSON, C., *Numerical solution of partial differential equations by the finite element method* (Studentlitteratur, Lund, 1987).

[18] KAHNG, B., BATROUNI, G., REDNER, S., DE ARCANGELIS, L., AND HERRMANN, H., *Electrical breakdown in a fuse network with random, continuously distributed breaking strengths*. Phys. Rev. B **37** (1988) 7625–7636.

[19] KANTOR, Y. AND WEBMAN, I., *Elastic properties of random percolating systems*. Phys. Rev. Lett. **52** (1984) 1891–1894.

[20] KELLOMÄKI, M., *Rigidity and transient wave dynamics of random networks*, Ph.D. Thesis, University of Jyväskylä (1998).

[21] KITTEL, C., *Introduction to solid state physics* (Wiley, 1957), 2nd ed.

[22] KÄHKÖNEN, S., ÅSTRÖM, J., AND TIMONEN, J. To be published.

[23] LAI, W., RUBIN, D., AND KREMPL, E., *Introduction to Continuum Mechanics*, No. 17 in Pergamon engineering series (Pergamon Press, 1973).

[24] LANDAU, L. AND LIFSCHITZ, E., *Theory of elasticity, Course of theoretical physics* (Pergamon Press, 1970).

[25] LATVA-KOKKO, M., *Statistical physics of rigidity and elasticity in random structured materials*, Ph.D. Thesis, University of Jyväskylä (2002).

[26] MAXWELL, J., *On the calculation of the equilibrium and stiffness of frames*. Phil. Mag. **27** (1864) 294299.

[27] MÄKINEN, J., *The mechanical and geometrical properties of fibrous structures*, Ph.D. Thesis, University of Jyväskylä (2001).

[28] NECAS, J. AND HLAVACEK, I., *Mathematical theory of elastic and elastoplastic bodies: An introduction*, No. 3 in Studies in applied mechanics (Elsevier, 1981).

[29] NISKANEN, K. AND ALAVA, M., *Planar random networks with flexible fibers*. Phys. Rev. Lett. **73** (1994) 3475–3478.

[30] NISKANEN, K., NILSEN, N., HELLEN, E., AND ALAVA, M., *KCL-PAKKA: Simulation of the 3d structure of paper*, in *The Fundamentals of Papermaking Materials, Transactions of the 11th Fundamental Research Symposium*, edited by C. Baker (PIRA International, 1997), vol. 2.

[31] Numerical algorithms group, *NAG fortran 77 library Mark 18 manual*.

[32] OBUKHOV, S., *First order rigidity transition in random rod network*. Phys. Rev. Lett. **74** (1995) 4472–4475.

[33] PAGE, D. AND SETH, R., *The elastic modulus of paper II. The importance of fiber modulus, bonding and fiber length*. Tappi **63** (1980) 113–116.

[34] PIKE, G. AND SEAGER, C., *Percolation and conductivity: A computer study I*. Phys. Rev. B **10** (1974) 1421–1434.

[35] RÄISÄNEN, V., *Numerical models for reversible and irreversible deformations of disordered media*, Ph.D. Thesis, Helsinki University of Technology (1997).

[36] RÄISÄNEN, V., ALAVA, M., AND NIEMINEN, R., *Failure of planar fiber networks*. J. Appl. Phys. **82** (1997) 3747–3753.

[37] RÄISÄNEN, V., ALAVA, M., NISKANEN, K., AND NIEMINEN, R., *Does the shear lag model apply to random fiber networks?* J. Mater. Res. **12** (1997) 2725.

[38] SAITO, Y., UEMARA, H., AND UWAHA, M., *Two-dimensional elastic lattice model with spontaneous stress*. Phys. Rev. B **63** (2001) 045422–1–9.

[39] SEAGER, C. AND PIKE, G., *Percolation and conductivity: A computer study II*. Phys. Rev. B **10** (1974) 1435–1446.

[40] STAUFFER, D. AND AHORANY, A., *Introduction to percolation theory* (Taylor & Francis, 1994).

[41] STENULL, O. AND JANSSEN, H., *Multifractal properties of resistor diode percolation* (2001). ArXiv cond-mat/0110560.

[42] VINNURVA, J., ALAVA, M., ALA-NISSILÄ, T., AND KRUG, J., *Kinetic roughening in fiber deposition*. Phys. Rev. E **58** (1998) 1125–1131.

[43] VOGEL, S., *Cat's paws and catapults. Mechanical worlds of Nature and People (in finnish, translated by Kimmo Pietiläinen)* (Terra Cognita, 2001).

[44] VOSS, H., *Iterative methods for linear systems of equations, Textbook of the* 3^{rd} *International Summerschool, Jyväskylä, Finland*, No. 27 in Lecture Notes (University of Jyväskylä, Department of Mathematics, 1993).

[45] WILHELM, J. AND FREY, E., *Elasticity of stiff polymer networks* (2003). ArXiv cond-mat/0303592.

[46] WOLFF, J., *The law of bone remodelling* (Springer-Verlag, 1986).

[47] YOUNG, D., *Iterative solution of Large Linear System* (Academic Press, 1971).

[48] ZHOU, Z., LAI, P.-Y., AND JOÓS, B., *Rigorous solution for the elasticity of diluted gaussian spring networks*. Phys. Rev. E **62** (2000) 7490–7493.

[49] ÅSTRÖM, J., LATVA-KOKKO, M., KÄHKÖNEN, S., MÄKINEN, J., AND TIMONEN, J., *The role of connectivity in the properties of sedimented materials*. Granular Matter **5** (2003) 99–103.

[50] ÅSTRÖM, J., MÄKINEN, J., ALAVA, M., AND TIMONEN, J., *Elasticity of poissonian fiber networks*. Phys. Rev. E **61** (2000) 5550.

[51] ÅSTRÖM, J., MÄKINEN, J., ALAVA, M., AND TIMONEN, J., *Erratum: Elasticity of poissonian fiber networks*. Phys. Rev. E **62** (2000) 5862.

[52] ÅSTRÖM, J., MÄKINEN, J., HIRVONEN, H., AND TIMONEN, J., *Stiffness of compressed fiber mats*. J. Appl. Phys. **88** (2000) 5056.

[53] ÅSTRÖM, J., SAARINEN, S., NISKANEN, K., AND KURKIJÄRVI, J., *Microscopic mechanics of fiber networks*. J. Appl. Phys. **75** (1994) 2383–2392.

Appendix A

Floyd's algorithm

We begin by defining few basics of graph theory. A graph is a collection of vertices and edges. Each edge has one or two vertices associated with it. These vertices are called the endpoints of the edge and the edge connects these vertices. A graph is a tree if it contains no loops. A loop means that there is a set of edges that takes one from some vertex back to itself without visiting any vertex or edge twice. We can now represent our random fibre network as a graph where each contact point of fibres is a vertex and each fibre segment is an edge.

Our task is to find shortest paths in a network. Given a directed, weighted network $G = (V, E, l)$, where V is the set of all vertices, E is the set of lines which defines the connectivity between vertices, i.e. the edges, and l is the given set of weights for edges (in our case the lengths of fibre segments). It is valid to assume that a weight associated with each of the edges in E is equal to or greater than zero. For simplicity we also assume that all of the G's nodes are numbered as $V = 1, 2, \ldots, n$. Our task is to find the shortest distance between all node pairs $(i, j) \in E$,

$$D[i, j] = \text{the shortest path from } i \text{ to } j.$$

Here the length of the path $i \xrightarrow{e_1} k_1 \xrightarrow{e_2} \ldots \xrightarrow{e_{t-1}} k_{t-1} \xrightarrow{e_j} j$ is defined as a sum of the lengths of the edges:

$$l(e_1, \ldots, e_t) = \sum_{s=1}^{t} l(e_s). \tag{A.1}$$

A solution method for the given problem is to create a queue of $n \times n-$arrays $D_k, k = 1, \ldots, n$, in a such way that $D_k[i, j]$ is the length of the shortest path from vertex i to j through vertices $1, \ldots, k$. Clearly we see that $D[i, j] \equiv D_n[i, j]$.

Arrays D_k can created by recursion in the following way:

$$D_0[i,j] = \begin{cases} 0 & \text{if } i = j; \\ l(i,j) & \text{if } i \neq j \text{ and } (i,j) \in E; \\ \infty & \text{otherwise.} \end{cases} \tag{A.2}$$

$$D_k[i,j] = min(D_{k-1}[i,j], D_{k-1}[i,k], D_{k-1}[k,j]), k \geq 1. \tag{A.3}$$

From above we get the following algorithm [2,3].

Algorithm 1 [Floyd]
for k=1 to n do
  for i=1 to n do
    for j=1 to n do
      $D[i,j] = \min(D[i,j], D[i,k] + D[k,j])$
return D

The algorithm returns an array with elements containing the lengths of the shortest paths from every vertex to another. From the group of boundary vertices we still have to find the shortest one. As such we only get the *length* of the shortest path, but by adding a reference array inside the for-loops, we also get the actual path. The time requirement for the algorithm is of the order of $O(n^3)$.